TAMPEREEN TEKNILLINEN YLIOPISTO
TAMPERE UNIVERSITY OF TECHNOLOGY

MARI LEHTI-POLOJÄRVI

ELECTRICAL IMPEDANCE TOMOGRAPHY APPLIED TO STEM CELLS IN HYDROGEL SCAFFOLD

Master of Science Thesis

Examiners: professor Jari Hyttinen, postdoctoral researcher Edite Figueiras and postdoctoral researcher Niina Onnela
Examiners and topic approved in the Faculty of Computing and Electrical Engineering council meeting on June 4th 2014

ABSTRACT

MARI LEHTI-POLOJÄRVI: Electrical impedance tomography applied to stem cells in hydrogel scaffold
Tampere University of Technology
Master of Science Thesis, 72 pages, 3 Appendix pages
December 2014
Master's Degree Programme in Electrical Engineering
Major: Medical Physics
Examiners: Professor Jari Hyttinen, postdoctoral researchers Edite Figueiras and Niina Onnela

Keywords: Electrical impedance spectroscopy, electrical impedance tomography, gellan gum hydrogels, stem cells, sensitivity field

There is a great need for new imaging methods for monitoring cell growth in the fields of tissue engineering and regenerative medicine. Electrical impedance tomography (EIT) could provide a label free, non-invasive and fast method for cell culture monitoring. This thesis is a feasibility study on what kind of results EIT may provide when cells are cultured in a 3D hydrogel scaffold.

This thesis is divided into two parts: (1) electrical impedance spectroscopy (EIS) measurements and (2) computer modelling of the EIT setup. In the EIS study part, several different gellan gum (GG) hydrogels, with and without encapsulated stem cells are measured using the impedance spectroscope HF2IS device (Zurich Instruments AG, Switzerland). The impedance spectrum of GG hydrogel samples, cell culture medium samples and a combination of them are measured. EIS measurements are done to samples with different amounts of adipose stem cells: 0.5 million, 1 million and 2 million. The cell viability is also measured by EIS. In the second study part, two dimensional EIT computer models are done in COMSOL Multiphysics. The sensitivity field of EIT setup is simulated in order to find the optimal electrode locations and resistivity values for the aqueous solution used between electrodes and the sample.

The EIS experiments indicate that the impedance value is dependent on the amount and viability of cells. The average impedance for 0.5 million cells in 1 ml of GG hydrogel incubated in 1 ml of cell culture medium drops 13 % after samples are exposed to lethal 43 °C temperature for 2 hours. Optimal electrode configuration and resistivity values are obtained by the EIT model and these parameters can be used in the future EIT measurements. The results suggest that EIS can be used as a tool for assessing cells encapsulated in 3D hydrogel scaffold. However, further studies are needed to assess the role of the cell culture medium on the determination of the amounts of cells. In order to enhance the statistical significance of the viability results, additional samples should be measured.

TIIVISTELMÄ

MARI LEHTI-POLOJÄRVI: Impedanssitomografia sovellettuna kantasoluihin hydrogeeli skaffoldissa
Tampereen teknillinen yliopisto
Diplomityö, 72 sivua, 3 liitesivua
Joulukuu 2014
Sähkötekniikan diplomi-insinöörin tutkinto-ohjelma
Pääaine: Lääketieteellinen fysiikka
Tarkastajat: professori Jari Hyttinen, tutkijatohtorit Edite Figueiras ja Niina Onnela

Avainsanat: Sähköinen impedanssispektroskopia, sähköinen impedanssitomografia, gellan gum hydrogeeli, kantasolut, sähköinen sensitiivisyys kenttä

Uusille solujen kasvua monitoroiville menetelmille on suuri tarve kudosteknologian ja regeneratiivisen lääketieteen aloilla. Impedanssitomografia (EIT) voisi tarjota merkkiaineettoman, ei-invasiivisen ja nopean tavan monitoroida solujen kasvua. Tämä työ on toteutettavuustutkimus siitä millaisia tuloksia impedanssitomografialla olisi mahdollista saavuttaa soluista, joita kasvatetaan 3D hydrogeeli skaffoldissa.

Työ jakaantuu kahteen osaan: (1) impedanssispektroskopia (EIS) mittauksiin ja (2) tietokone simulaatioihin EIT-mallilla. Ensimmäisessä osassa mitataan erityyppisten näytteiden impedanssi useilla eri taajuuksilla HF2IS impedanssispektroskopia laitteistoa (Zurich Instruments AG, Switzerland) käyttäen. EIS mittaus tehdään gellan gum (GG) hydrogeelille, solunkasvatus mediumille sekä näiden yhdistelmälle. Lisäksi mitataan rasvankantasoluja, joita kapseloidaan hydrogeeliin eri määriä: 0.5, 1 ja 2 miljoonaa. Näiden mittausten perusteella valitaan solujen määräksi 0.5 miljoonaa näytteisiin, joista mitataan elävien ja kuolleiden solujen vaikutusta impedanssiin. Työn toisessa osassa tehdään 2D tietokone malli EIT järjestelmästä COMSOL Multiphysics -ohjelmalla. Sensitiivisyyskenttää simuloidaan EIT-mallilla, jotta löydetään optimaalisin elektrodien sijainti sekä resistiivisyysarvo vesiliuokselle, jota on näytteen ja elektrodien välissä.

Työn tulokset osoittavat, että mitattu impedanssin arvo riippuu solujen määrästä ja siitä ovatko solut eläviä vai kuolleita. Keskimääräinen impedanssi 0.5 miljoonalle solulle 1 ml GG hydrogeelissä viljeltynä 1ml solunkasvatus mediumia tippui 13 %, kun näytteitä altistettiin tappavalle 43 °C lämpötilalle kahden tunnin ajan. EIT simulaatioiden perusteella on mahdollista löytää optimaalisin vesiliuoksen resistiivisyysarvo sekä elektrodien sijainti. Simuloituja parametreja voidaan käyttää jatkossa EIT mittauksissa. Tulosten perusteella EIS mittauksia voidaan käyttää solujen tutkimiseen 3D hydrogeeli skaffoldissa. Lisätutkimuksia tarvitaan solunkasvatus mediumin vaikutuksesta solumäärien mittaukseen sekä lisänäyttöä parantamaan tilastollista varmuutta elävien ja kuolleiden solujen vaikutuksesta mitattuun impedanssiin.

PREFACE

This thesis is part of the Human Spare Parts project at the Institute of Biosciences and Medical Technology, BioMediTech. The work was performed at the Department of Electronics and Communications Engineering at Tampere University of Technology.

Professor Jari Hyttinen is the examiner and postdoctoral researchers Edite Figueiras and Niina Onnela are the supervisors of this thesis. Jari Hyttinen is the originator of most grand ideas and has managed the evolving of the whole project. Edite Figueiras leads the project group in which this work is a part of. She has been involved in all possible practical stages and given valuable support and ideas. Niina Onnela is an expert in bioimpedance measurements and has been irreplaceable guide in the development and analysis of the EIS system and its results.

This thesis is done in collaboration with Biomaterials and Tissue Engineering group led by Professor Minna Kellomäki at Tampere University of Technology and Adult Stem Cell Group led by Docent Susanna Miettinen at University of Tampere. The measured hydrogel samples are provided by Janne Koivisto, Jette-Britt Naams and Ana Soto de la Cruz. Jyrki Sivula has been responsible for cell culturing.

I would like to thank all parties I have had the pleasure to work with. In addition to all above-mentioned contributors, I am grateful to Jenny Parraga Meneses for hydrogel expertise, Aku Seppänen for the practical tips at Jyväskylä summer school and Aapo Tervonen, Narayan Puthanmadam Subramaniyam and Daniel García León for COMSOL advice. Especially I wish to express my gratitude to the day care personnel and relatives who have taken excellent care of my children so I was able to concentrate on this thesis. Finally, a few words to my personal sparring partner: Kiitos Ville.

In Tampere, Finland, on 17 November 2014

Mari Lehti-Polojärvi

TABLE OF CONTENTS

SYMBOLS AND ABBREVIATIONS

AC	Alternating current
ASC	Adipose stem cell
CC	Refers to current carrying couple formed by CC1 and CC2 electrodes
CC1, CC2	Current carrying electrodes
DC	Direct current
EIS	Electrical impedance spectroscopy
EIT	Electrical impedance tomography
FEP	Fluorinated ethylene propylene
GG	Gellan gum
GG-1.1SPM	Gellan gum hydrogel cross-linked with 1.1 % w/v of SPM
GG-0.6SPM	Gellan gum hydrogel cross-linked with 0.6 % w/v of SPM
OM	Optical microscopy
PU	Refers to pick-up couple formed by PU1 and PU2 electrodes
PU1, PU2	Pick-up electrodes, refers to voltage measurements electrodes
SPM	Spermine
SPD	Spermidine
2D	Two dimensional
3D	Three dimensional
w/v	Mass/volume percentage (%)
A	Cross-sectional area of a volume conductor (m^2)
C	Capacitance (F)
C_m	Capacitance of cell membrane (F)
E	Complex voltage (V)
G	Total gain of current amplifier HF2TA (V/A)
I	Complex current (A)
I_Z	Current through an object with impedance Z (A)
$\boldsymbol{J}_{LE}$	Current density field produced by reciprocal energization of voltage measurement electrodes ($1/m^2$)
$\boldsymbol{J}_{LI}$	Current density field produced by current excitation electrodes ($1/m^2$)
L	Inductance (H)
N	Amount of cells in cell gradient samples
P	Operator representing the function of measured value and value of interest, refers to g
R	Resistance (Ω)
R_C	Contact resistance (Ω)
R_e	Resistance of extracellular material (Ω)
R_G	Transimpedance gain of current amplifier HF2TA (V/A)
R_i	Resistance of intracellular material (Ω)
R_m	Resistance of cell membrane (Ω)
R_1	Resistance of a resistor in the reference RC circuit (Ω)
R_2	Resistance of a resistor in the reference RC circuit (Ω)
S	Sensitivity ($1/m^4$)
V_{final}	Volume of the final particle/cell-hydrogel-cell culture medium suspension (m^3)
$V_{solution}$	Volume of the solution prior mixing (m^3)

$V_{spheres}$	Volume of suspended spheres (m^3)
V_Z	Voltage across an object with impedance Z (V)
X	Reactance (Ω)
Z	Impedance (Ω)
Z_C	Impedance of a capacitor (Ω)
Z_L	Impedance of an inductor (Ω)
Z_s	Stray Impedance (Ω)
d	Measured inner diameter of the FEP tube (m)
f	Frequency (Hz)
g	Unknown function of interest, refers to inverse problem
h	Total length of the cylindrical sample (m)
i	Imaginary unit
l	Length of the volume conductor, in this thesis, the distance between electrode tips (m)
l_p	Length of the slime mold *Physarum polycephalum*, illustrated in figure 2.6 (m)
$\boldsymbol{m}$	Indirect measurement of a function g
n	Noise and measurement errors
r	Distance between sample center and electrode center in EIT model (m)
$r_{spheres}$	Radius of a spherical particle or cell (m)
s	Length of the arc of the circle (m)
s_{inner}	Length of the arc of the circle, refers to electrodes next to y-axis in neighboring method (m)
v	Volume of the volume conductor (m^3)
w	Width of the slime mold *Physarum polycephalum*, illustrated in figure 2.6 (m)
x	Cartesian x-axis
x_1, x_2, x_n	Measured variables in function u
y	Cartesian y-axis
Φ	Volume fraction (%)
α	Angle between r and y-axel in EIT model
θ	Phase angle (°)
ρ	Resistivity (Ωm)
σ	Conductivity of suspension (S/m)
σ_1	Conductivity of suspending medium (S/m)
σ_2	Conductivity of suspended spheres (S/m)
ω	Angular frequency (Hz)
Δd	Accuracy of measurement of variable d (m)
Δl	Accuracy of measurement of variable l (m)
ΔR	Accuracy of measurement of variable R (Ω)
$\Delta\rho$	Maximum error of a function ρ
Δu	Maximum error of a function u
$\Delta x_1, \Delta x_2, \Delta x_n$	Accuracy of measurement of variable x_1, x_2, x_n

1. INTRODUCTION

Research in the fields of tissue engineering and regenerative medicine aims to provide new techniques for the regeneration, replacement and repair of lost or damaged tissues. Thus providing new hope for patients with, for example, bone, neuron or cardiac dysfunctions [1]. Therapeutic approaches based on the combination of stem cells and biomaterials in a three dimensional (3D) graft to be implanted or used as a preclinical tissue model, are a potential source for new therapies [2]. Hydrogels are one potential 3D scaffold for growing stem cells and is proven to maintain cell viability and differentiation capability [2], [3]. Tissue engineering applications include interfaces between biomaterials, cells and tissues and result in challenges concerning monitoring and assessing results. Thus, there is a great need for new imaging methods for monitoring the cell growth [1].

Electrical impedance spectroscopy (EIS) is a powerful method for characterizing electrical properties of materials [4]. EIS involves measuring the impedance of a system over a range of frequencies. It is a high speed, non-invasive technique that has been applied to characterizing the dielectric properties of biological cells [5].

Simplifying the electrical properties of biological cells, they consist of a conducting cytoplasm with nucleus covered by a thin insulating membrane. The cell membrane behaves like a capacitor: insulating low frequencies of alternating current (AC) electric field and passing high frequencies [5]. This means that the size and shape of the cell can be obtained by measuring the electrical properties at low frequencies. At high frequencies the internal properties (cytoplasmic resistance) can be probed [6], [7].

There are several EIS studies of single cells or cell aggregates [8]–[10] and cells growing on a 2D electrode chip [10]–[12]. EIS has been demonstrated as a useful technique for monitoring adhesion (bonding), spreading and motility of anchorage-dependent cells [12], [13]. It has been applied to sorting dead cells from living cells and counting them [9]. However, 2D cultures provide very different growing environment than *in vivo*, lacking the cell-cell and cell-matrix interactions [13]. Also direct contact between cells and electrodes can lead to the damage of cells due to the local high electric field intensity and Joule heating effect [7]. Thus moving into 3D culturing and monitoring of cells is set as a first priority. Even though there are plenty of EIS studies of biological cells, there are only few of measuring cells and especially stem cells in a 3D hydrogel scaffold [14].

EIS provides information plotted, for example, in impedance-frequency plane, but electrical impedance tomography (EIT) is a method for producing 2D or 3D images. These images represent the electrical conductivity distribution of the measured region. [15]. The great opportunities of EIT are due to the fact that it is noninvasive, fast and low cost. The major drawback is its poor spatial resolution. Thus EIT has been concerned as an application of detecting conductivity changes rather than absolute conductivity values [5], [15].

In medical field EIT has not yet reached a breakthrough into mainstream clinical practice. [16]. However, there are several proof of principle studies and steady progress in many fields. For example, imaging breast cancer and brain function are promising techniques for clinical use. EIT has also been used for cell cultures [7], [17]. The great advantage of using impedance measurements in cell cultures is that labelling is not needed for detecting cell viability [13]. Thus EIT would enable the analysis of physiological state of cells.

The goal of this thesis is to provide initial information about the electrical properties of the 3D hydrogel samples and to produce a plan of an EIT setup. The work is divided into two parts: spectroscopic measurements of different types of samples and a computer model of EIT setup in 2D. The first part is theoretically EIS and it includes measuring the basic properties of the bulk material where the cells are grown, that is, blank hydrogel, cell culture medium and they combined. Then the needed amount of cells is defined first by measuring alumina particles and then with real living cells. To obtain a reference for the future research, samples with living cells are exposed to lethal 43 °C to induce dead cells. These samples are measured before and after the heat exposure. The second part includes optimizing the electrode locations and choosing a good resistivity value for the aqueous solution between electrodes and the cylindrical sample.

2. THEORETICAL BACKGROUND

EIS is a method for obtaining frequency dependent impedance information of a sample under study. EIT is a method for reconstructing images illustrating the internal resistivity distribution of a sample. This chapter introduces the principles behind these methods. First, stem cells and gellan gum (GG) hydrogels are briefly presented. Then, electrical impedance and how it can be measured and analysed are discussed. Finally, different EIT methods and how they can be assessed using lead field theory are presented.

2.1 Stem cells

Stem cells are cells that have two special properties: ability to renew themselves in an undifferentiated stage and differentiate into many cell types [18]. They can be harvested from multiple sources, such as embryos, bone marrow and stem cell populations of different organs and tissues [19]. According to their differentiation capacity, stem cells can be divided into three main groups: 1) totipotent cells, such as a fertilized egg or an early embryo, which are able to form a new individual, 2) pluripotent cells can differentiate into any cell type of any organ and 3) multipotent stem cells, which are more limited in their differentiation capacity [20].

Human embryonic stem cells are in the first group and they have nearly unlimited developmental potential. They can be used for transplantation therapies or for different *in vitro* models. The drawbacks are their limited availability, ethical issues and their probability of causing tumors. Human induced pluripotent stem cells are in the second group of stem cells. They were originally derived from adult human cells, such as fibroblasts, and reverted to the stem cell stage by gene transduction. [20]

Even though the third group of stem cells is limited in their differentiation capacity, they are clinically interesting because they carry a smaller risk of forming tumors compared to cells of embryonic origin [20]. One type of multipotent stem cells is adipose stem cells (ASC). They can be harvested from an adult tissue, for example fat tissue. Easy availability of ASCs makes them suitable for tissue engineering studies, thus they are used in this study [21].

2.2 Gellan gum hydrogels

Gellan gum (GG) is an extracellular polysaccharide, secreted by bacteria *Sphingomonas elodea*. GG forms a soft physical gel by undergoing a random coil to double helix

transition upon cooling. To form stronger gel, cations need to be present as GG solution is heated and cooled down. There are different types of cations which are used as cross-linking agents. One option is to use, for example, calcium or magnesium cations. [22], [23] Another way is to use biological amines such as spermidine (SPD) or spermine (SPM) [24].

GG hydrogels have been widely used in the food industry as a stabilizer and thickening agent, but recently also as a scaffold in culturing mammalian cells for tissue engineering applications [23], [24]. GG hydrogel cross-linked with SPD has been proven to be suitable for cell culture [24]. The hydrogels used in this work are cross-linked with SPM, which is a similar type of amine as SPD.

GG hydrogels provide a 2D or 3D scaffold with properties very similar to living tissues [24]. They allow the diffusion of nutrient and signaling molecules both to and from the cells encapsulated within the hydrogel [23]. They are also stable to temperature changes [22]. Transparency of GG hydrogels makes them feasible to be imaged optically.

2.3 Electrical impedance and resistivity

Electrical impedance means the total opposition that a circuit or material under study presents to an alternating current (AC). In a direct current (DC) case, one can refer to resistance. Alternating current or voltage consists of two independent elements: magnitude and phase. Therefore, impedance needs to be dealt with an extended version of the Ohm's law: $Z = E/I$, where Z is impedance, E voltage drop and I applied current and all values are complex numbers. Impedance can be further expressed either in the rectangular coordinate form (2.1) or in the polar coordinate form (2.2) as follows

$$Z = R + iX \tag{2.1}$$

$$Z = |Z|e^{i\theta} \tag{2.2}$$

where R is resistance, i is the imaginary unit, X is the reactance and θ is the phase angle. Thus impedance is a vector quantity that can be illustrated, for example, as in figure 2.1. [25]

Resistance R is the real part of the complex impedance. It is a constant value for a certain measured circuit or material, which means that it does not depend on the frequency applied, even though temperature or other physical factors can change it. Reactance X consists of capacitive and inductive elements. They are dependent on the applied frequency and on the circuit property inductance L or capacitance C. The impedance of a capacitor decreases as frequency increases, since $Z_C = 1/(j\omega C)$, where $\omega = 2\pi f$ and f is the frequency. On the other hand, impedance of an inductor is $Z_L = j\omega L$, implying that the impedance of an inductor increases as frequency increases. Reactance elements have a property to store and emit energy and resistance elements

dissipate it. Phase angle θ is the angle between the voltage E and current I, which depends on the value of reactance in the circuit. For purely resistive system the phase angle is zero. [25]

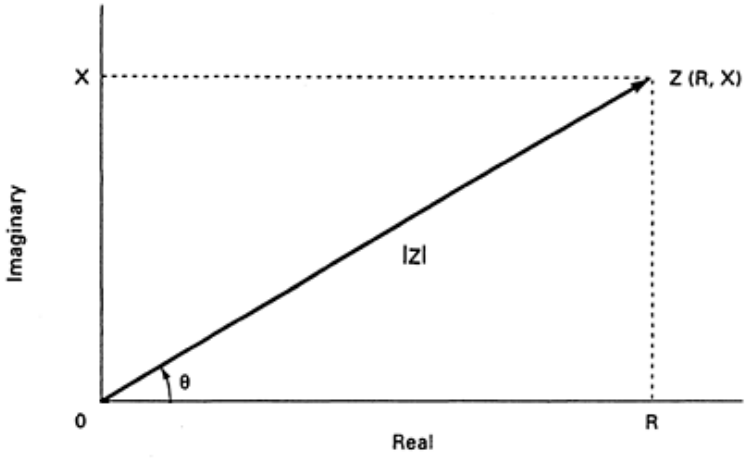

Figure 2.1. *An impedance vector Z represented on the complex plane at a certain frequency. Resistance R is the real part of impedance and reactance X is the imaginary part of the impedance. Phase angle θ is the angle between the impedance vector and the real axis. Adapted from* [25].

Impedance depends on both the electrical properties of the sample and the measuring system geometry but resistivity is a material constant independent of its dimensions. Resistivity ρ can be calculated from the real part of the measured impedance R as follows

$$\rho = R \cdot \frac{A}{l} \tag{2.3}$$

where A is the cross-sectional area of the conductor and l is the length of the conductor. The unit of resistivity is Ωm. The inverse of resistivity is conductivity σ with units S/m. [5], [26].

Electrical resistivity or conductivity of a mixture of materials can be mathematically calculated. One approach is to calculate the electrical conductivity of a suspension of spheres as follows

$$\frac{(\sigma/\sigma_1)-1}{(\sigma/\sigma_1)+2} = \Phi \frac{(\sigma_2/\sigma_1)-1}{(\sigma_2/\sigma_1)+2} \tag{2.4}$$

$$\xrightarrow{yields} \sigma = \frac{\sigma_1(2\Phi a+1)}{1-\Phi a} \tag{2.5}$$

where

$$a = \frac{(\sigma_2/\sigma_1)-1}{(\sigma_2/\sigma_1)+2} \tag{2.6}$$

and σ, σ_1 and σ_2 are specific conductivities of the suspension, the suspending and the suspended spheres respectively. In addition, Φ is the volume fraction of the suspended spheres. It can be calculated as follows

$$\Phi = \frac{V_{spheres}}{V_{solution}} \cdot 100 \tag{2.7}$$

where $V_{spheres}$ is the total volume of encapsulated spheres and $V_{solution}$ is the sum of all constituents in the solution prior mixing with the spheres [27]. For example, if there are particles encapsulated into hydrogel, σ would be the conductivity of the mixture, σ_1 the conductivity of the hydrogel and σ_2 the conductivity of the particles. Equation (2.6) is substituted into equation (2.4) and equation (2.5) is solved from it. Equation (2.5) can be used to calculate the conductivity (or resistivity by using the inverse values of conductivity) of the total suspension σ as a function of volume fraction Φ. The motivation for this theory is to model the conductivity of blood and it holds only for homogenous spheres in a dilute suspension [28].

2.4 Electrical impedance spectroscopy

In EIS an electrical stimulus, either known voltage or current, is applied to the electrodes and the response (resulting voltage or current), is then measured. When the stimulus is done over a range of frequencies, the frequency dependent information can be obtained. As impedance can be calculated according to the current and voltage data, EIS represents the impedance over a certain frequency range. It is assumed that the system itself is time invariant during the measurement. [4]

Typical ways of representing results of EIS are Bode and/or Nyquist plots. Bode plot consist usually of two graphs, one representing the magnitude of impedance $|Z|$ as a function of frequency f, and the other, phase angle θ as a function of frequency. For pure capacitor, the phase angle is -90°, for pure resistor it is 0° and for *RC* circuit somewhere in between, depending on the frequency. This can be seen in figure 2.2, representing the spectrum of a parallel *RC* circuit. Bode plot represent impedance magnitude and phase angle usually on a wide range of frequencies, other values on a logarithmic scale, except phase. An advantage of Bode plot is a good visualization of all frequency responses. [4]

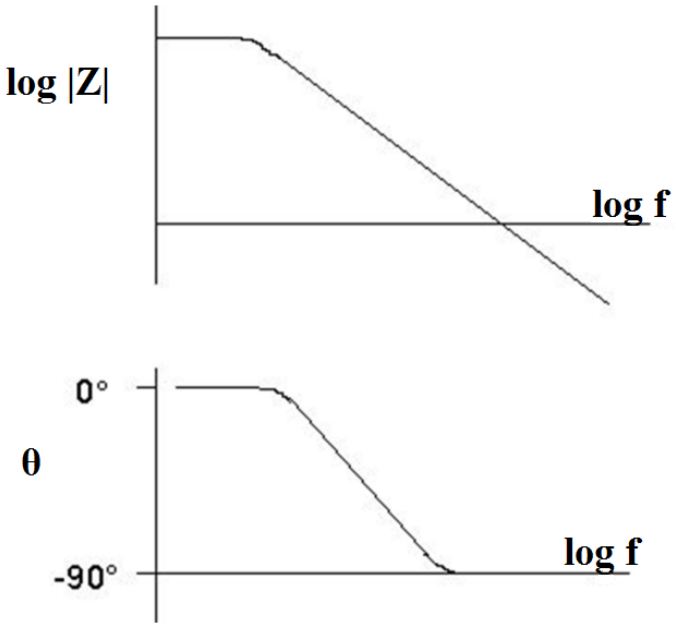

Figure 2.2. *Bode plot of the complex impedance for a parallel RC circuit. Impedance magnitude |Z| and phase θ decrease as frequency increases because capacitor impedance reduces. Impedance magnitude and frequencies f are represented on a logarithmic scale. Adapted from* [29].

Nyquist plot would be another commonly used way of representing the complex impedance behavior. The imaginary part of the impedance is plotted as a function of the real part of the impedance for a range of frequencies. From Nyquist plot, it is easy to determine some important values, such as circuit resistance *R*, from the intercepts of the real axis. The disadvantage is that the frequency information of impedance is difficult to distinguish from the Nyquist plot. [4]

Data analysis of EIS measurement results can be based either on mathematical model or on equivalent circuit of the electrode sample system. In either case, the parameters can be estimated and the measured impedance compared to the theoretical one. The analysis of EIS results can be ambiguous. The problem in analyses based on equivalent circuit is that the circuit elements represent ideal properties. As again the behavior of real tissue engineering samples can be far from the ideal lumped constants. [4]

2.5 Four-terminal measurement technique

Impedance of an unknown object can be measured using two, three or four connections to the object. A setup consisting of only two electrodes in contact with the sample is called a two-terminal measurement. An example of a two-terminal setup is shown in figure 2.3. This setup is simple to implement but contains some measurement errors. First, there might exist some stray impedance originating from cable impedances, labeled as Z_s in figure 2.3. Second, there is a contact resistance, labeled as R_c in figure

2.3, at each contact points between the sample and the cable. The contact resistance can be several ohms and it can be unstable. These factors cause a significant error to the measurement result if the sample impedance is relatively small. Thus the two-terminal measurement is used mainly for the measurement of high impedance materials when the cable impedance is not significant. [4], [5], [25]

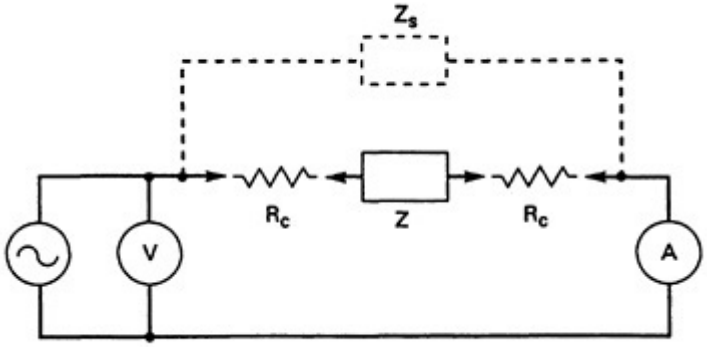

Figure 2.3. *The two-terminal measurement of an unknown impedance Z. There is an AC power supply, voltmeter, ammeter and the sample being measured.* R_c *stands for contact resistance and* Z_s *for possible stray impedance. Adapted from* [25].

Three-terminal measurement is used to solve the first above-mentioned problem, which is the stray impedance. Then a third electrode is used for voltage measurement. However, three-terminal setup measures the differential voltage between the voltage electrode and the current electrode including the contact impedance of the current electrode. The four-terminal measurement is therefore usually preferred if sample impedance is less than some kΩs. [25]

Four-terminal measurement eliminates also the contact impedances. In a 4-terminal setup, two electrodes are used as current injection electrodes and two electrodes as voltage measurement electrodes. A four-terminal setup is represented in figure 2.4. The voltmeter has high input impedance and minimal amount of current is dissipated into the voltage measurement circuit. Thus the voltage across the sample, between points A and B in figure 2.4, can be measured with high accuracy.

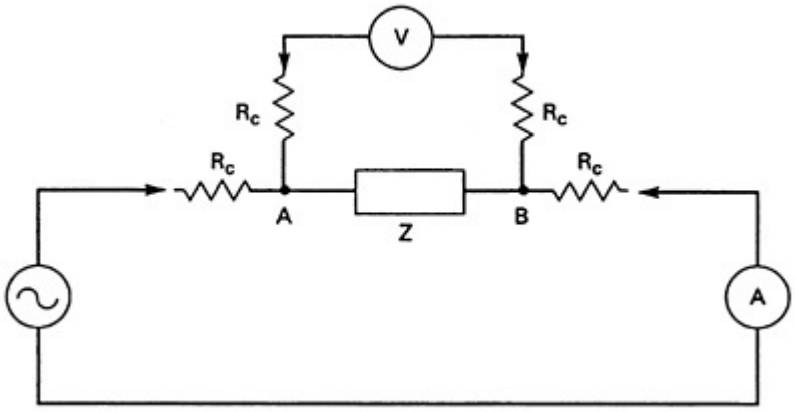

Figure 2.4. *The four-terminal measurement of an unknown impedance Z. The circuit is otherwise similar to figure 2.3, but the voltmeter is connected directly to the sample using additional wires. Adapted from* [25].

Especially when measuring low impedance samples, it is important to use the 4-terminal measurement. It might be impossible to differentiate the impedance of the sample if it is of the same magnitude as the impedances of electrode connections and cables.

2.6 Hydrogels and biological cells as electrical conductors

There are two mechanisms how electrical current can flow in a material: ionic and electronic, or the mixture of these. In ionic currents, the charge carriers are free ions that migrate according to the voltage difference. If charge carriers are electrons, as in metals, the ions of the material are immobilized. [5] Because ionic currents means transport in the material, an externally applied direct current (DC) will change the conductor, first near the electrodes and with longer time also in the bulk of the material.

Impedance of GG hydrogels have been studied, for example, in order to find the gelation temperature of calcium cross-linked GG [30]. It was shown that impedance increases as the GG solution cools down and shows a knee as the solution is gelated at about 36 °C. After GG solution is gelated, the impedance continues increasing as the temperature decreases. This is a sign that the ion mobility decreases as the GG gelates and cools down [30].

There are several studies of different types of hydrogels showing high impedance or resistivity values. In the previous example, the calcium cross-linked GG had an impedance value of about 1.2 kΩ at 36 °C, measured with two electrodes of distance 2.5 cm and averaged at 100 Hz – 100 kHz [30]. Agar gel (1.5 % in distilled water) has shown a resistivity value of 56.5 Ωm [7]. The impedance of Poly-hydroxyethyl methacrylate hydrogels with different cross-linker concentrations was measured using two electrodes. [31]. The reported resistivity range was as huge as 1000-17000 Ωm

depending on the cross-linker concentration. They assume this is because of the decrease in average molecular weight between cross-linkers, which creates a stiffer structure with smaller pores.

The impedance of biological cells has been extensively studied. Single cells [7], [8], [10], cell clusters [10], [11], cells on a 2D plate [7], [10], [12], [32] or in 3D suspension or tissue [33], [34] have all been studied. There is also some studies of cells in a 3D hydrogel scaffold [14]. In order to understand how millions of biological cells, either separately or in clusters, affect the impedance of the whole sample, the basics of cells in electric field are briefly introduced.

When electric current is passed through a sample containing cells, the current propagation is divided into two different paths as is represented in figure 2.5. One path runs only in the extracellular material rounding the cells. The other path propagates straight through the cells. This behavior can be explained with an equivalent circuit consisting of resistors and capacitors. The extracellular material is now assumed to be fluid and is represented by the resistance R_e, which is mainly dependent on the ionic composition of the fluid. The other branch of the equivalent circuit is more complex, since it crosses the cell membrane two times and the cytoplasm. The cell membrane can be modeled as a parallel connection of a capacitor and a resistor with capacitance C_m, and resistance R_m, respectively. The cytoplasm is represented by resistance R_i. [6]

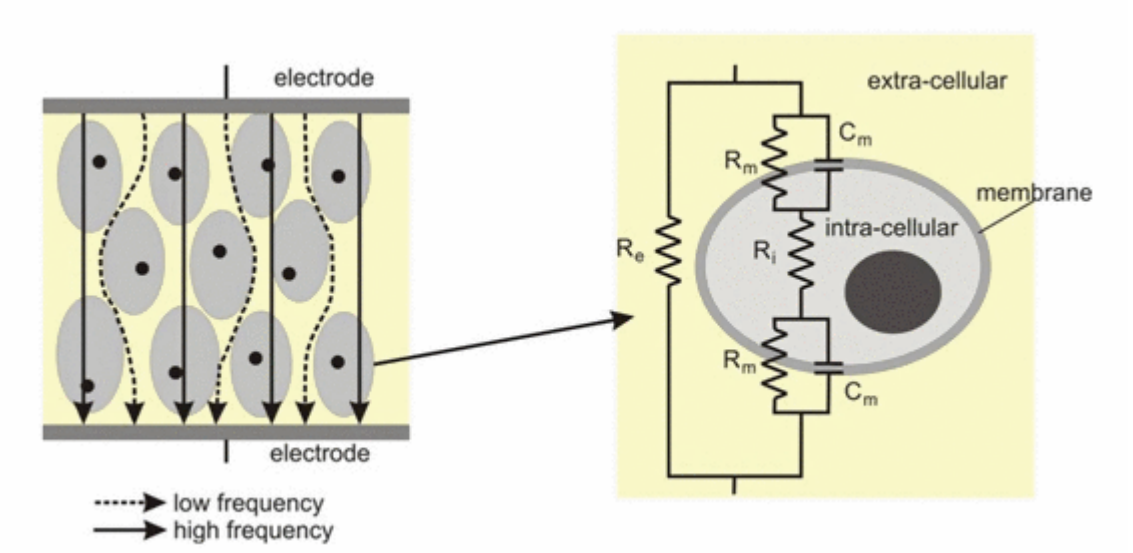

Figure 2.5. *Left: current propagation at high (solid line) and low frequencies (dotted line) through a cell culture. Right: equivalent electrical circuit of a biological cell. R_e denotes extracellular resistance, R_m membrane resistance, R_i intracellular resistance and C_m membrane capacitance. [6]*

At low frequencies, the capacitor C_m acts like an open circuit and most of the current flows through the resistive parts R_e, R_m and R_i of the circuit. The membrane resistance R_m is typically in the range of MΩ which is usually significantly larger than R_e. This

results in the flow of the current through extracellular material. At high frequencies, the capacitor C_m acts like a short circuit. The alternating electric potential is then transmitted through C_m into the intracellular volume where the resulting current is limited by R_i. The leakage current of the membrane contributes only a small portion, so R_m can usually be ignored. Thus, the total current is essentially composed of the membrane capacitance C_m and cytoplasmic resistance R_i in parallel with extracellular resistance R_e. The relative contributions depend on the packing density of the cells and the ionic compositions of the cytoplasm and extracellular material. [6]

Then, one can make the question what are the above-mentioned low and high frequencies, that is, at which frequency the cell membrane capacitance allows current flow? According to Klösgen et al., at frequencies less than 1 MHz, the conductivity of biological tissue is determined by the conductivity of the electrolyte in the extracellular space. [6]. Then the total conductivity depends on the volume of the extracellular space. At certain frequencies in the range of 100 kHz-10MHz, depending on the material under study, the impedance of the cell membrane can be ignored. Thus, impedance should decrease at frequencies 100 kHz-10 MHz, because the cell membrane becomes conductive.

Studies of living cells have shown that cells are very poor conductors below 10 kHz [35]. A single cell study of yeast cells shows that the cell membrane is opaque to electrical field still at 200 kHz but at 5 MHz cell membrane is transparent to electrical field [9]. Thus, the change happens above 200 kHz for yeast cells with radius of approximately 4 µm. A combination of a large living cell (amoeboid plasmodium of the slime mold *Physarum Polycephalum* with width and length of several mm) and agar gel has been measured by EIS and imaged by EIT [7]. The EIS measurement was done between frequencies 1 kHz-1 MHz. A decrease in impedance and a negative phase is shown at frequencies below 100 kHz, but above this, the impedance is stable and also phase angle approaches zero. These studies suggest that there can be great differences on the capacitance of the cell membrane. This can be a result of the cell size: smaller cells start conducting at higher frequencies than large cells [36].

Measured impedance is different in living and dead cells [9]. Living cells have undamaged membrane thus all above-mentioned aspects can be applied. However, the membrane of dead cells is ruptured allowing electrical current to pass directly through the cytoplasm. In addition, living cells have more conducting cytoplasm than dead cells. [9], [37] At low frequencies, when the membrane is not conducting, the impedance of dead cells is lower than living cells. At high frequencies, when current passes through cytoplasm, dead cells express higher impedance than living cells.

2.7 Electrical impedance tomography

In EIT several electrodes, typically placed on the surface of the sample, are used to measure the impedance. In practice several four-terminal measurements are done probing the whole volume of interest. EIT aims to produce images related to the conductivity or resistivity distribution of the measured region. These images are reconstructed according to the known stimulation current and measured voltage data. In practice, the reconstruction techniques are sensitive to noise and small errors in the measured data cause large errors in the resulting images. Thus the sensitivity and selectivity of the measurement should be maximized in the area of interest. [15]

According to the lead field theoretical approach, any change in the conductivity of a region produces a change in the impedance signal that is proportional to the relative amount of current flowing in that region [38]. Thus a change in the conductivity, changes the distribution of the introduced current in the volume conductor as well. An example of a reconstructed EIT image is illustrated in figure 2.6, where a biological cell (slime mold *Physarum Polycephalum*) is encapsulated on the agar gel in an EIT chip. The cell is seen as a dark area in the image, indicating Physarum cell to be more conductive than the agar gel.

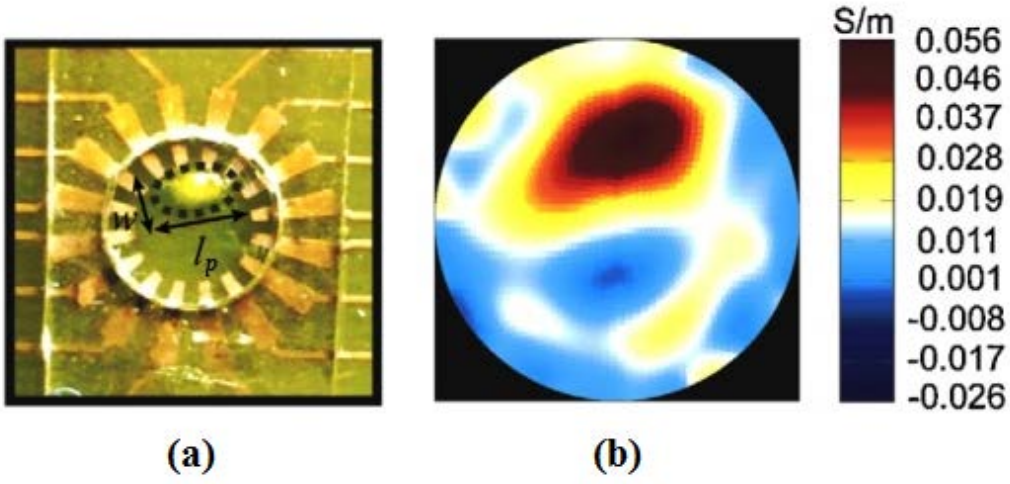

Figure 2.6. *(a) Optical image of a Physarum polycephalum cell on the agar gel in an EIT chip. The width of the cell is w = 1.61 mm and the length is l_p = 3.19 mm. (b) Reconstructed EIT image of the setup in (a). The color bar represents the conductivity of the EIT image. Adapted from [7].*

Theoretically EIT is an inverse problem: image is reconstructed according to finite number of boundary measurements of an unknown object [7]. In general terms, solving an inverse problem means recovering the cause when the effect is known. In practice, this means usually interpreting indirect measurements (***m***) of an unknown function of interest (*g*). This can be expressed as an equation ***m*** = P*(g)* + *n*, where P is an operator representing the function of measured value and value of interest and *n* models the noise

and other measurement errors. If operator P^{-1} does not exist or is not continuous, we are dealing with ill-posed inverse problem, which EIT is. Several algorithms have been developed to solve and regularize the inverse problem. They include, for example, maximum a posterior approach and Monte Carlo sampling method. [7], [39]

In biomedical field, solving EIT inverse problem can mean, for example, solving the electrical properties of biological cells or cell clusters in order to gain knowledge about their physiological properties. One property that is under intensive study at the moment is to determine the cell viability, since living cells possess different electrical properties compared to dead cells.

2.7.1 Sensitivity field

The capacity of an EIT measurement to detect resistivity and its changes in a region of interest can be evaluated by calculating the sensitivity in that region. Sensitivity *S* is the relation of the measured impedance caused by a given resistivity distribution. It describes how effectively each region contributes to the measured impedance. Selectivity is the proportional value of the sensitivity in the target region against the total sensitivity over the sample. In order to optimize the signal obtained from a certain region, both sensitivity and selectivity of the measurement should be maximized in that region. [15]

For a four-terminal measurement, the measured macroscopic impedance Z of an inhomogeneous sample is calculated as [38]

$$Z = \int_v \rho \boldsymbol{J}_{LE} \cdot \boldsymbol{J}_{LI} dv \tag{2.8}$$

where ρ is resistivity of each region, v is volume and $\boldsymbol{J}_{LE}$ and $\boldsymbol{J}_{LI}$ are current density fields associated with the voltage measurement and current injection leads. Thus both measurement and current feeding electrodes and their locations equally define the measurement sensitivity distribution. These current density fields are based on the reciprocity theorem. According to the theorem, the relationship between excitation and response remains unchanged when the points of excitation and response are interchanged. Then the measured impedances are equal. This requires that the sample is linear and passive. [38]

If the sample is homogeneous, resistivity can be taken out of the integral. The sensitivity *S* for each voxel can be expressed as

$$S = \boldsymbol{J}_{LE} \cdot \boldsymbol{J}_{LI} \quad [1/m^4] \tag{2.9}$$

Sensitivity can be positive or negative depending on the directions of the current density fields. Thus the measured impedance can increase, decrease or be unaffected by a resistivity change in a particular region. In a volume conductor, there are negative and

possible zero sensitivity values depending on the electrode setup that complicate the image reconstruction. [15]

2.7.2 Measurement strategies in EIT

There are different data acquisition methods for EIT and four of them are presented: neighboring, opposite, cross and adaptive [38], [40]. An example of each is visualized in figure 2.7, where the most sensitive measurement of the center of the sample is chosen. The visualizations of the methods are presented in [40].

Neighboring method uses two adjacent electrodes for current feeding and the voltage is measured by other two adjacent electrodes circulating the whole sample. Then current feeding is moved one step and voltage measurement is done similarly. This is repeated until the whole circle is scoped. This method is most sensitive near the electrodes and least sensitive in the center.

In the **opposite** method, current is injected through diametrically opposed electrodes. Voltage is measured with one electrode next to current feeding electrode and the other circulating the whole object. Then current circuit is moved to next location and the same pattern repeated until the whole sample is scoped. Only lower voltage electrode is changing place at one acquisition while others have fixed locations.

The **cross** method uses more distant electrodes instead of the adjacent ones. First, two adjacent electrodes are selected as current and voltage reference. Then the voltage measurement is taken from each location and after each scanning, the current electrode is moved. This is repeated when the first electrodes are moved.

In the **adaptive** method, current is injected through all electrodes. As many independent current generators are needed as are electrodes used. Voltage is measured on all electrodes keeping the other at fixed place according to current feeding position. The adaptive method produces most homogenous sensitivity throughout the model.

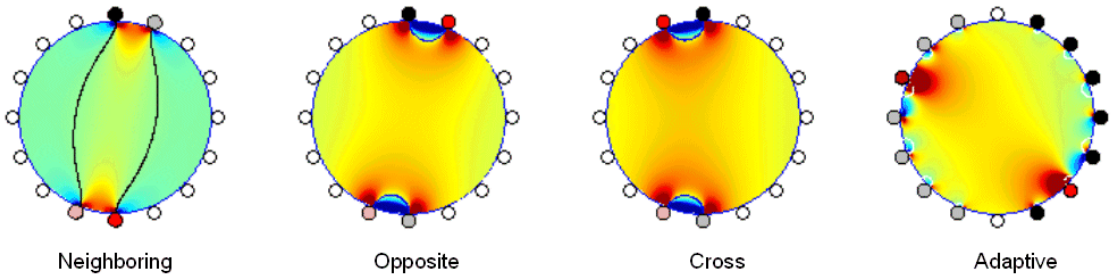

Figure 2.7. *The most sensitive configurations to detect center region of the model. Black circles are locations for current carrying electrodes and red circles for voltage detection. The sample is modeled homogenous and symmetric. [40]*

The sensitivity of the last three methods is relatively similar compared to neighboring method, which is less sensitive in the center. Typically, in EIT setups electrodes and sample are stationary, and they are in contact with each other. The aim of this work is to find the best and practically feasible measurement strategy for a setup where the electrodes are not in contact with the sample. In addition, only certain sections of the circumference are available for electrode placement. Thus a modified method of above-mentioned methods is required.

3. RESEARCH MATERIALS AND METHODS

Materials and methods used in this thesis are divided into two parts: the ones used in the EIS measurements and the ones used in the EIT computer models. First, samples and measurement setup used in the EIS are presented. Then, the EIT models and used parameters are discussed. The resistivity value obtained from EIS measurements is chosen to be used in the EIT simulations.

3.1 EIS measurements

The idea of measuring EIS instead of moving on straight to the EIT imaging is to obtain knowledge of the frequency behaviour of the hydrogels and hydrogels with encapsulated cells. This is similar to what has been done for example in [7], where the results of EIS are used to choose a suitable frequency for EIT. In addition, the EIS results provide resistivity information from the sample that can be applied to computer models or used for assessing the EIT images.

The EIS measurement setup is designed, optimized and built using the Zurich impedance spectroscopy instrumentation system (HF2IS, Zurich Instruments AG, Switzerland). The electrode shape and material is first examined. Then a setup for holding electrodes is designed and 3D printed. Suitable voltage and frequency values are decided according to literature review of similar type of samples. The setup is tested with a reference *RC* circuit to be sure that the connections and settings are good.

3.1.1 Materials for EIS samples

Two slightly different GG hydrogel compositions are used in this thesis: GG-1.1SPM and GG-0.6SPM. Both are cross-linked with SPM but with different concentrations. In GG-1.1SPM, there is 1.1 % w/v of SPM and in GG-0.6SPM there is 0.6 % w/v of SPM. The hydrogels are made from GG (Gelzan^{TM} CM - Gelrite ®, G1910, Sigma Aldrich, Saint Louis, USA) and SPM (Spermine tetrahydrochloride, BioUltra, for molecular biology, ≥ 99.5 % (AT), 85605, Sigma Aldrich, Saint Louis, USA) solutions, both dissolved in water with 10 % sucrose (Sucrose – BioXtra, ≥ 99.5 %, S7903, Sigma Aldrich, Saint Louis, USA) content. These solutions are heated to +37°C and then mixed using a pipette. The mixing and gelation is done in a cylindrical fluorinated ethylene propylene (FEP) tube covered with parafilm in the lower part.

The used alumina (aluminium oxide Al_2O_3 ,Albemarle Corporation, Martoxid® DN-206) is a white powder that is insoluble in water. The powder contains three different

size ranges of the particles with cumulative distribution: 1 – 3 µm (10 %), 5 – 7 µm (50 %) and 10 – 20 µm (90 %). There is maximum 3 % of the powder with particles bigger than 45 µm. Alumina is electrically an insulator with resistivity of 10^{12} Ωm [41]. Bulk density reported by the manufacturer is 750 kg/m^3.

Human adipose stem cells (ASCs) are encapsulated into hydrogel. The cells are harvested and cultured at Regea (BioMediTech, Tampere, Finland). The size of these ASCs vary significantly from 6 µm to 100 µm [42]. These samples are prepared with a known number of cells, and are then incubated for at least 24 hours. During this time the cells have probably attached to the gel and proliferated, so the actual amount of cells being measured is probably higher than the amount of cells inserted in the gels. The typical electrical conductivity of a cell membrane is around 10^{-7} S/m that of the cytoplasm can be as high as 1 S/m. If a cell dies, the membrane becomes permeable and conductivity increases by a factor of about 10^4. [43]

Cell culture medium is used to feed the cells before and after encapsulation into hydrogel. It is a solution with several components. ASCs are cultured in Dulbecco's modified Eagle's medium DMEM/F-12 1:1 (Life Technologies, Rockville, MD) supplemented with 1% L-analyl-L-glutamine (GlutaMAX I; Life Technologies), 1% antibiotics (p/s; 100 U/ml penicillin, 0.1 mg/ml streptomycin; Lonza, Walkersville, MD) and either 10% FBS (Life Technologies) or 5% HS (human serum type AB; Lonza). The same medium is inserted on top of the hydrogel after cell encapsulation. In this thesis, there are three separate measurements including ASCs encapsulated into hydrogel: (1) preliminary cell measurements, (2) cell gradient measurements and (3) viability measurements. For the first two measurements, cell culture medium with FBS is used, but for the third measurement, FBS serum is replaced by HS serum. This difference is due to practical reasons. However, the effect of different serums on the average size or growth rate are minimal and should not affect comparability of the results [42]. For the preliminary and viability measurements, ASCs are detached by scraping in order to form clusters. For the cell gradient measurements, ASCs are detached using TrypLE Select (Life Technologies) producing a single cell suspension.

3.1.2 Measured samples

Most samples are a mixture of previously mentioned materials, making some of them rather complex. Contents and preparation of the samples are explained below in the same order as they are presented in chapter 4.1. All samples are prepared into FEP tubes of diameter 1 cm and kept in upright position until the EIS measurements. This allows the cell culture medium to diffuse into the hydrogel. Concerning all samples containing ASCs, Jyrki Sivula is responsible of growing the cells and Janne Koivisto prepared the cell-hydrogel samples.

The samples, labeled as GG-1.1SPM and GG-0.6SPM, are called **blank hydrogels** since they contain only GG and cross linker SPM. First, three samples of GG-1.1SPM are measured using three different volumes: 1 ml, 1.5 ml and 2 ml. They are kept in fridge for three days before measurements. Then, five parallel samples of both blank hydrogel types are measured. The sample volume is chosen to be 1.5 ml according to the first measurements. These samples are measured during the same day as being prepared but samples are kept at room temperature at least two hours before measurements to be sure gelation has finished. The blank hydrogels are made by Janne Koivisto and Ana Soto de la Cruz.

Five parallel samples of cell culture medium solution with 1.5 ml volume are measured. In this measurement, only DMEM/F-12 is measured, missing the more expensive ingredients: antibiotics, serum and L-analyl-L-glutamine.

Samples with 1 ml of cell culture medium (only DMEM/F-12) inserted on top of blank hydrogel after gelation are named **bulk samples**. Five parallel bulk samples with 1.5 ml of GG-1.1SPM and 1 ml of cell culture medium are measured. They are incubated for 24 hours at 37 °C before measurements. These samples are made by Jette-Britt Naams. In addition, some bulk samples are prepared as a control for samples containing alumina particles or cells, as it is explained below.

Five different concentrations of alumina particles encapsulated into 1.3 ml of GG-0.6SPM are tested and one bulk sample as a control. To make the samples comparable with cell samples, 1 ml of cell culture medium (only DMEM/F-12) is inserted. The concentrations of alumina particles are: 0.5 mg/ml, 1 mg/ml, 2 mg/ml, 3mg/ml and 4 mg/ml. Particles are first suspended into 50 µl of purified water and then mixed into hydrogel. Samples are made by Janne Koivisto and they are incubated for 24 hours at 37 °C before measurements.

Preliminary cell samples consist of approximately 375 000 ASC in 1ml of GG-0.6SPM and 1 ml of cell culture medium on top of the gel. Three parallel samples are measured. The cells are partly in clusters and partly as single cells. After the cells are encapsulated into the hydrogel, they are incubated for two days in 37 °C before EIS measurements.

Cell gradient measurements include different amounts of encapsulated ASCs in 1 ml of GG-1.1SPM and 1ml of cell culture medium. The original amount of cells are: 0.5 million, 1 million and 2 million ASCs in 1ml of hydrogel and one bulk sample is prepared as a control. There is one sample of each, except two parallel samples of 1 million cells. The cells are encapsulated as single cells into the hydrogel and incubated for three days at 37 °C before EIS measurements

In the viability measurements, 0.5 million of ASCs organized in clusters are encapsulated into 1 ml of GG-0.6SPM and 1 ml of cell culture medium. Four parallel samples with cells and four parallel bulk samples are measured. For practical reasons,

the EIS measurements of these eight samples is divided into two days: two cell samples and two bulk samples are measured after three days of incubating and the rest after four days of incubating at 37 °C.

3.1.3 Measurement setup

Electrodes which are suitable for measuring 3D GG hydrogel on a wide frequency range are first chosen. There are two main aspects to take into account: the material and the shape of the electrode. According to preliminary studies in chapter 4.1.1, Ag-AgCl electrodes are not stable with GG hydrogel, thus more noble metal is chosen. Other options are gold and platinum. Gold is commonly used as electrode material in hydrogel and cell culture studies [7], [12], [31]. Platinum is also used, for example, on cell culture chip [17]. It is known to be good in AC work but poor in DC studies [44], which suits well for EIS measurements. For this application, the shape of the electrode could be, for example, plate or stick electrodes. Plate electrodes would generate a homogenous electrical field. However, because this is a starting step towards EIT, stick electrodes are chosen instead of plates. Thus, platinum stick electrodes are used in this work with dimensions of 1 mm x 0.5 mm x 15 mm and they are made of full platinum (Labor-Platina Ltd, Hungary).

The electrodes need to be placed so that they stay in place and the position is similar in each measurement. In addition, the placement of electrodes should be as minimally destructive as possible for the hydrogel sample. For this purpose electrode holders are designed using SolidWorks (Dassault Systèmes, SolidWorks Corp., version 2013) and 3D printed with Ultimaker Original (Ultimaker B.V., The Netherlands). A software, Cura (Ultimaker B.V., The Netherlands, version 14.01), is needed to adjust the 3D printing settings and to convert the designed model into GCode format. The printed material is polylactic acid (PLA) which is an electrically insulating and biodegradable plastic [45].

The designed electrode holder and its dimensions are represented in figure 3.1. It is a cylindrical piece with two rectangular holes for electrodes and a wall as an extrusion between the holes. The purpose of the wall is to help placing the holder in contact with the sample and to prevent accidental electrical contact of adjacent electrodes. The final dimensions are a result of trial and error, since they are dependent on the settings used in the 3D printer. The printing settings are set as high quality as possible to obtain exactly right sized holes for electrodes. A good hole size is found to be slightly larger than the electrode dimensions: 1.15 mm x 0.67 mm. Another crucial dimension is the diameter of the holder, which is set to 9.98 mm. If it was too big, it would not fit to the FEP tube, if it was too small the holder would not stay in place during the measurement. The depth of the holder is set to 7 mm because electrodes are 15 mm long. Thus this depth is enough to keep electrodes stable and there is still enough room for connecting the cables to the other end of the electrodes. Other dimensions illustrated in figure 3.1

proved to be practical but the exact dimensions are not crucial. In each measurement two similar holders are used in both ends of the FEP tube.

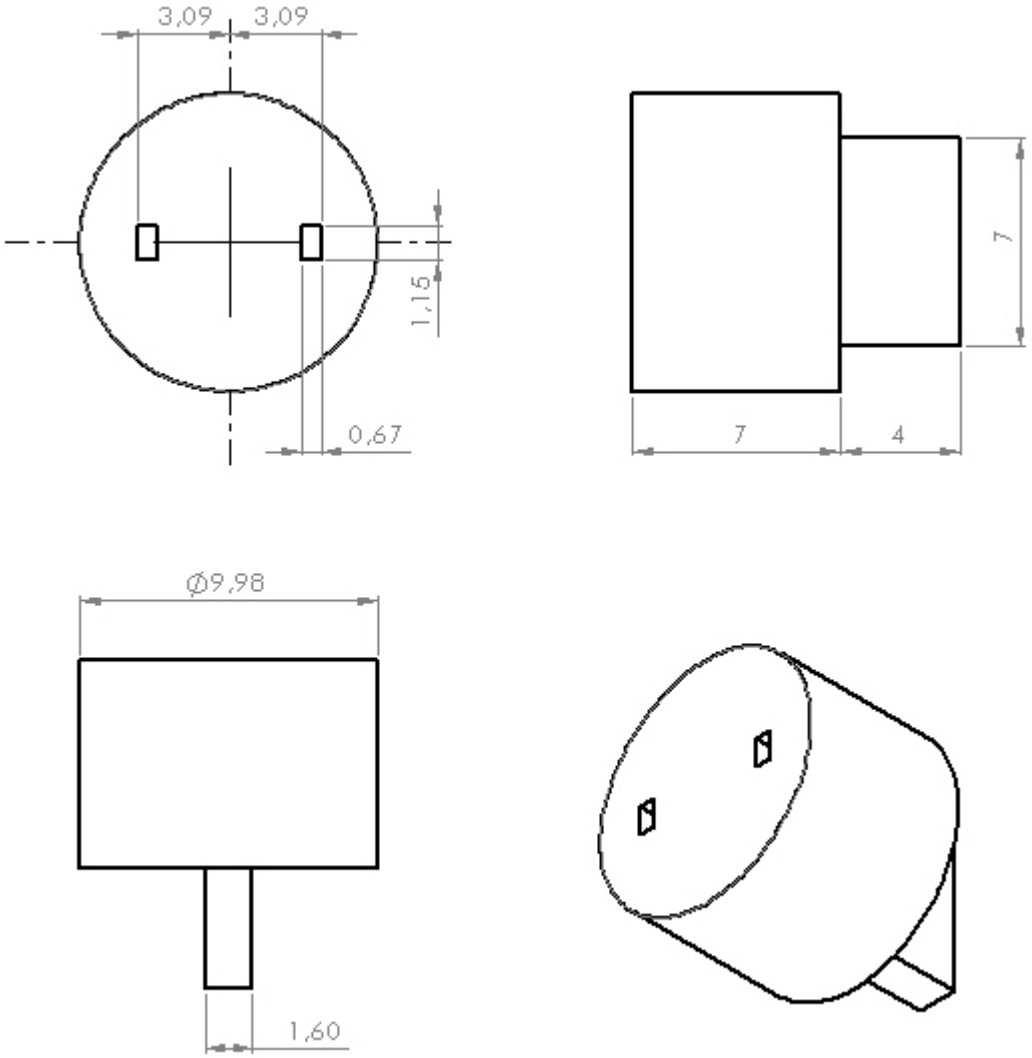

***Figure 3.1**. A design of the 3D printed holder from different angles. It is printed of PLA plastic with 100 % fill density. All dimensions are in mm.*

The sample is placed on a platform illustrated in figure 3.2. The platform is 3D printed similarly as the holder, but now the printing quality is not so crucial, for example, the fill density is now 20 %. Important dimension in the platform is the radius (5.50 mm) of the groove and that it is sunk into the platform a bit below the center of the origin of the groove. This keeps the tube, with outer diameter of 11 mm, in place during the measurement. The platform is taped on the shelf of the incubator. Several similar pieces of holders and platforms were 3D printed making it faster to measure multiple samples consecutively.

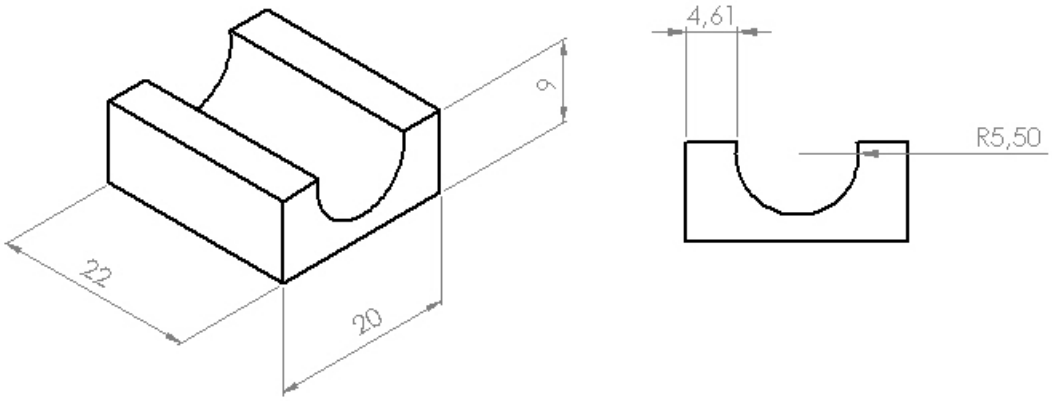

Figure 3.2. *A design of the 3D printed platform for samples in FEP tubes. Platform is printed of PLA plastic with 20 % fill density. All dimensions are in mm.*

The setup of sample, holders, platform and electrodes is represented in figure 3.3. The sample in the photo is one of the bulk samples. Electrodes CC1 and CC2 form the current circuit and PU1 and PU2 are used for voltage measurement. They are cross connected in order to enhance voltage sensing of the electric field. Dimension *h* is the length of the hydrogel volume and *l* is the distance between electrode tips. Both dimensions are controlled using a digital slide gauge. Electrodes are pushed 2 mm into the sample in each measurement. All measurements are done similarly, but the dimensions *l* and *h* depend on the sample volume.

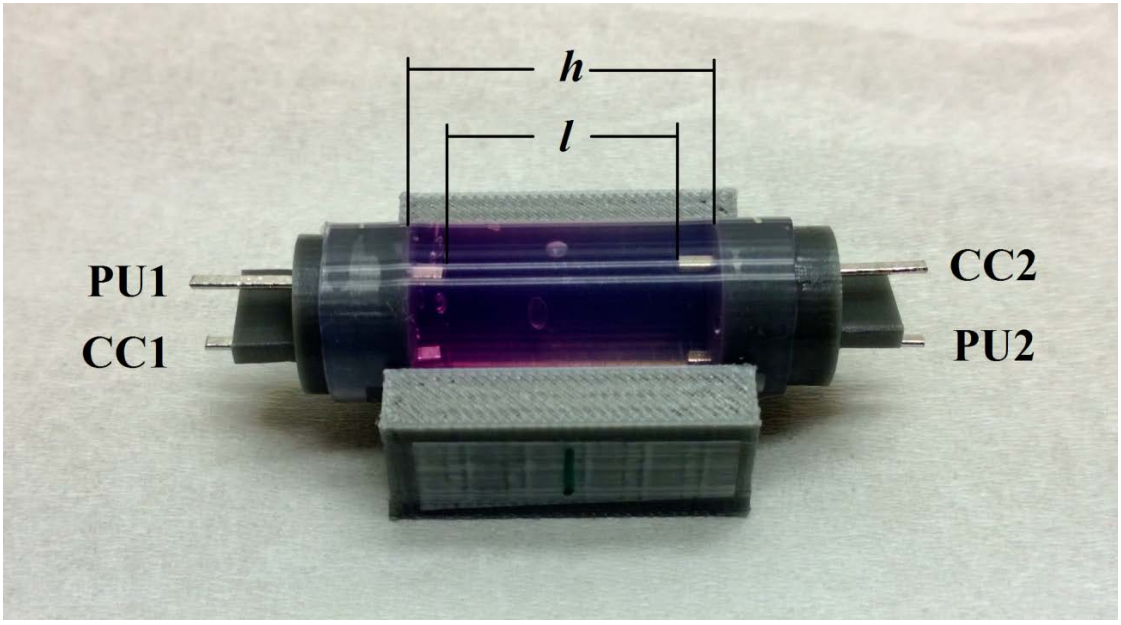

Figure 3.3. *Sample with holders and electrodes set on the platform. Electrodes CC1 and CC2 form the current circuit couple and PU1 and PU2 the voltage measurement couple. The dimension h is the length of the whole hydrogel volume and l is the distance between electrode tips. Electrodes are always pushed 2 mm into the sample, causing l to be 4 mm smaller than h.*

The HF2IS impedance spectroscope is used for signal generation and voltage measurement, and it is represented in figure 3.4. This system has two separate input and output channels and can operate on a frequency range from 0.7 µHz to 50 MHz [46]. For higher precision in the measurements, a current amplifier HF2TA (Zurich Instruments AG, Switzerland) can be used in conjunction with the HF2IS instrument. These components are controlled using a ziControl software (Zurich Instruments AG, Switzerland, version 14.02.23223).

Figure 3.4. *HF2IS Impedance Spectroscope manufactured by Zurich Instruments AG [46].*

According to the HF2 user manual [47] and the theory (chapter 2.5), when measuring impedances smaller than 10 kΩ, a four-terminal measurement is required. To obtain an accuracy in the range of 1 %, the circuit represented in figure 3.5, is used. The voltage V_Z across the sample *Z* is measured differentially by the *inputs 1+* and *1-* using 1 MΩ input impedance to prevent current dissipation in the measurement instrument. The

current I_Z through the sample is generated from *output 2* and directed through the current amplifier HF2TA to *input 2+*. Transimpedance gain R_G of 1k (V/A) and total gain G of 1k (V/A) are applied in the measurements. BNC cables, with length of 116 cm, are used in all connections, except the Ethernet cable between HF2IS and HF2TA and the USB 2.0 cable connecting HF2IS to PC.

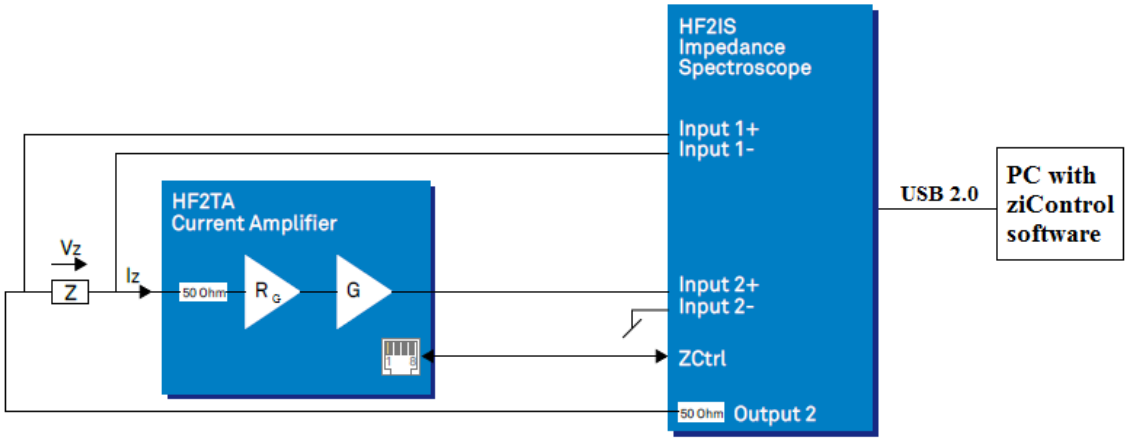

Figure 3.5. *Coupling circuit for four-terminal impedance measurement using HF2IS impedance spectroscope and HF2TA current amplifier. Z represents the sample being measured, V_Z is the voltage across the sample and I_Z is the current flowing through the sample generated by HF2IS. R_G represents transimpedance gain and G total gain of the HF2TA. ZiControl -software is used to control the measurements. Adapted from [47].*

The generated output signal is a sine wave with 25 mV amplitude. This amplitude is chosen according to previous studies on cell cultures or hydrogels that suggest to use small voltage in order to remain in the linear response region [7], [13], [48]. A frequency sweep is done from 10 Hz to 10 MHz because the cutoff frequency of HF2TA is 10 Hz and after 10 MHz results are not reliable. From this frequency range 100 data points are recorded. If averaging is applied in the frequency sweep, it is mentioned in the results.

The measured data is saved in CSV format, including frequencies at which the data points are taken and the impedance data (real and imaginary parts of impedance, phase angle and impedance magnitude). This data is then processed in MATLAB (MathWorks Inc., Natick, USA, version R2013a).

3.1.4 Measurement conditions

According to literature review, the impedance of hydrogels is dependent on the temperature [30], [49]. In order to keep measurement conditions as constant as possible, all EIS measurements are done at 37 °C. This temperature also supports the viability of the stem cells. The sample shown in figure 3.3, is placed inside the incubator (type B 8133, Termaks AS, Norway) during the measurements as is shown in figure 3.6.

Additionally a thermometer (Traceable® snap-in module with probe, Control Company, USA) is used to ensure the right temperature near the sample. Before each measurement, temperature is stabilized at least during 30 minutes.

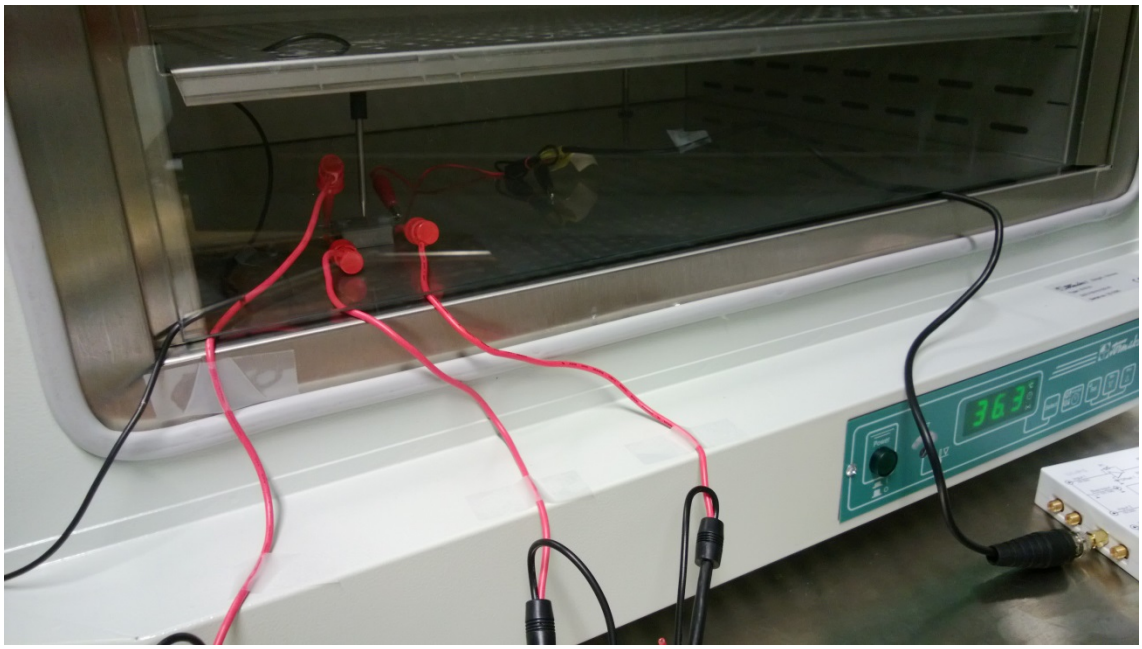

Figure 3.6. *Sample placed inside the incubator during measurements.*

Samples are measured at 37 °C right after they are received or incubated a certain time, as is explained in chapter 3.1.2. For the viability measurements each sample is measured at two different time points, before and after a lethal test. First, the EIS is measured at 37 °C, then samples are exposed to 43 °C for 2 hours in the incubator. Finally, EIS is measured again after the temperature is cooled back to 37 °C. It is expected that exposing cells to hyperthermia will cause the membrane to break, thus decreasing the measured impedance. The time and temperature for killing the cells is chosen according to previous studies, presented for example in [50]. Studies on Chinese hamster ovarian cells have shown that the rate of induced cell death at temperatures less than 42-43 °C is remarkably lower than above 43 °C. It is typical that death of cells is not linear according to the exposure time, but showing a shoulder which depends on the temperature. The higher the temperature, the less exposure time is needed to induce cell death. The GG hydrogel is assumed not to have irreversible effects by exposing it to 43 °C. This was anyhow measured by bulk samples, which were handled in the same way as samples with cells.

All parts which are in contact with the hydrogel are cleaned with distilled water and ethanol after and before use to avoid contamination. Most samples have originally 1 ml of cell culture medium on top of them but not all of it diffuses into the hydrogel. Thus the excess is carefully poured away before measurements. This is done at the same time for all samples to maintain the diffusion time as similar as possible to all samples.

3.1.5 Error estimation

Before each measurement the connections and settings are tested using a reference *RC* circuit. An equivalent circuit of the *RC* circuit used is illustrated in figure 3.7. The *RC* circuit has known parameters: R_1 = 475 Ω, R_2 = 442 Ω and C = 10 nF.

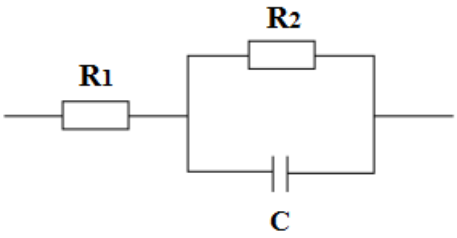

Figure 3.7. *Equivalent of the reference RC circuit used to test the connections and settings for the measurements: R_1 = 475 Ω, R_2 = 442 Ω and C = 10 nF.*

A measured and simulated frequency spectrums of the reference *RC* circuit are represented in figure 3.8. The simulation and the figure are done in the impedance analysis and equivalent circuit fitting program ZView (Scribner associates Inc., USA, version 3.20).

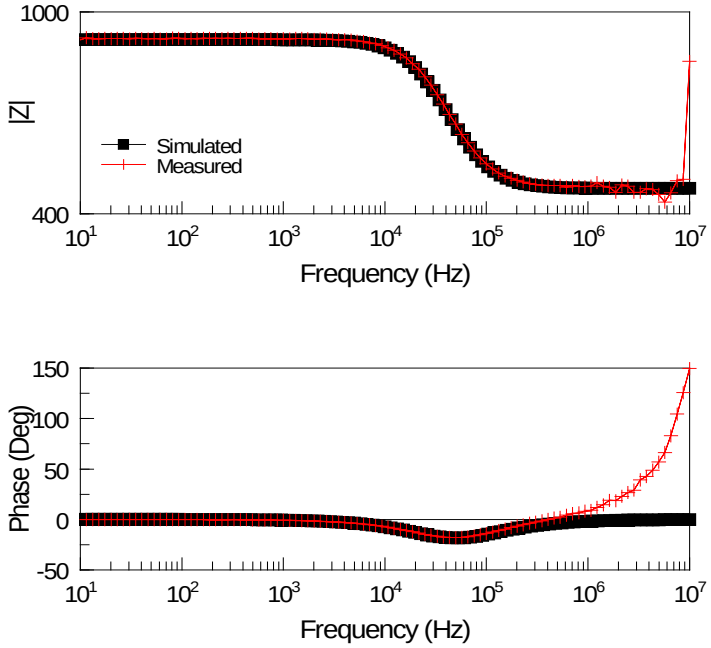

Figure 3.8 *Simulated and measured impedance spectrums of the reference RC circuit using 4-terminal measurement. No averaging is used in this measurement.*

The simulated and measured spectrums overlap until about 1 MHz. Above 1 MHz the impedance spectrum is noisy and above 5 MHz an inductive effect causes the impedance to increase strongly. The phase starts increasing after 1 MHz, which suggests that the inductance of cables and/or resistors affect the measured values. This is probably due to the fact that the length of the cables is approximately 116 cm.

Error of calculated resistivity values can be estimated by the maximum error of a function (Δu) as follows [51]

$$\Delta u \leq \left|\frac{\partial u}{\partial x_1}\right| \Delta x_1 + \left|\frac{\partial u}{\partial x_2}\right| \Delta x_2 + \cdots + \left|\frac{\partial u}{\partial x_n}\right| \Delta x_n \tag{3.1}$$

Resistivity ρ can be expressed applying $A = \pi(d/2)^2$ into equation (2.3), where A is the cross-sectional area of the FEP tube and d is the measured tube diameter, as follows

$$\rho = R\frac{A}{l} = R\frac{\pi d^2}{4l} \tag{3.2}$$

where R is the measured resistance and l measured distance between electrode tips (as is shown in figure 3.3). In all resistivity calculations, l is used instead of dimension h (see figure 3.3). This is because the used electrodes can be approximated as needle electrodes and for such, the highest electrical field strength is near the tip of the needle [5]. Equation (3.2) can be applied to equation (3.1), resulting

$$\Delta\rho \leq \left|\frac{\partial\rho}{\partial R}\right| \Delta R + \left|\frac{\partial\rho}{\partial d}\right| \Delta d + \left|\frac{\partial\rho}{\partial l}\right| \Delta l$$

$$= \frac{\pi d^2}{4l} \Delta R + \frac{R\pi d}{2l} \Delta d + \frac{R\pi d^2}{4l^2} \Delta l \quad (3.3)$$

where $\Delta\rho$ refers to the maximum error of calculated resistivity value and ΔR, Δd and Δl are the accuracies of measurements accordingly. In the case of several parallel samples are measured, errors can be estimated by calculating the standard deviation of the mean value.

3.2 EIT models

The voltage distribution inside a sample needs to be known in order to be able to do EIT image reconstruction. The reconstruction of the conductivity distribution requires usually measurement data from several current injection methods [52]. This would be problematic if the sample is not time-invariant, but in this work, samples can be assumed to be time-invariant. Our measurement model includes four electrodes on one side and two on the opposite side of the sample. This setup enables us to use a modified version of at least two different measurement strategies presented in chapter 2.7.2: the neighboring and the opposite. The neighboring method is expected to be good in scoping the boundary regions of the sample, but poor in the center regions. On the other hand, opposite method can be used for scoping the center areas of the sample. [40]

The EIT model is based on the finite element method (FEM), which is a computational technique to solve continuous real life problems by dividing the geometry into small finite-sized elements. The FEM modeling process consists of three parts: preprocessing, solution and postprocessing. In the preprocessing part, it is defined the geometry, material properties and boundary conditions. The solution part comprises the computation of the results. This can be done for example in COMSOL Multiphysics (COMSOL Ltd, version 4.3b) which is a FEM modeling based software. In the postprocessing part the results are analyzed and evaluated. [53]

The goal of the simulations is to optimize the resistivity parameters, the measurement strategy and the electrode locations. The initial values are obtained from EIS measurements at a resistive frequency area. The sample is assumed to be homogenous. In this application the electrodes are not in direct contact with the sample. To maximize the electric field and better sensitivity inside the sample, electrode distance from the sample is chosen to be as small as possible. In practice less than 1 mm might be difficult.

3.2.1 Geometry

The EIT model is built on the x-y plane in AC-DC module of COMSOL. The sample is modeled to be a circle with diameter of 10 mm placed at the origin. Electrodes are

modeled as 0.4 mm times 2 mm rectangles. The sample and electrodes are placed in a 50 mm times 50 mm rectangle, as is shown in figure 3.9 (a). The electrode location needs to be defined accurately, so the following equation is used [54]

$$s = \frac{\alpha}{360°} \cdot 2\pi r \tag{3.4}$$

where s is the length of an arc of a circle defined by an angle α and radius r, as is represented in figure 3.9 (b). Electrodes are placed in a circular position symmetrically around the sample. The coordinates of each electrode's center is defined using basic geometry as follows [54]

$$\begin{aligned} x &= r \cdot \cos(90° - \alpha) \\ y &= r \cdot \sin(90° - \alpha) \end{aligned} \tag{3.5}$$

where α is the angle between radius r and y-axis.

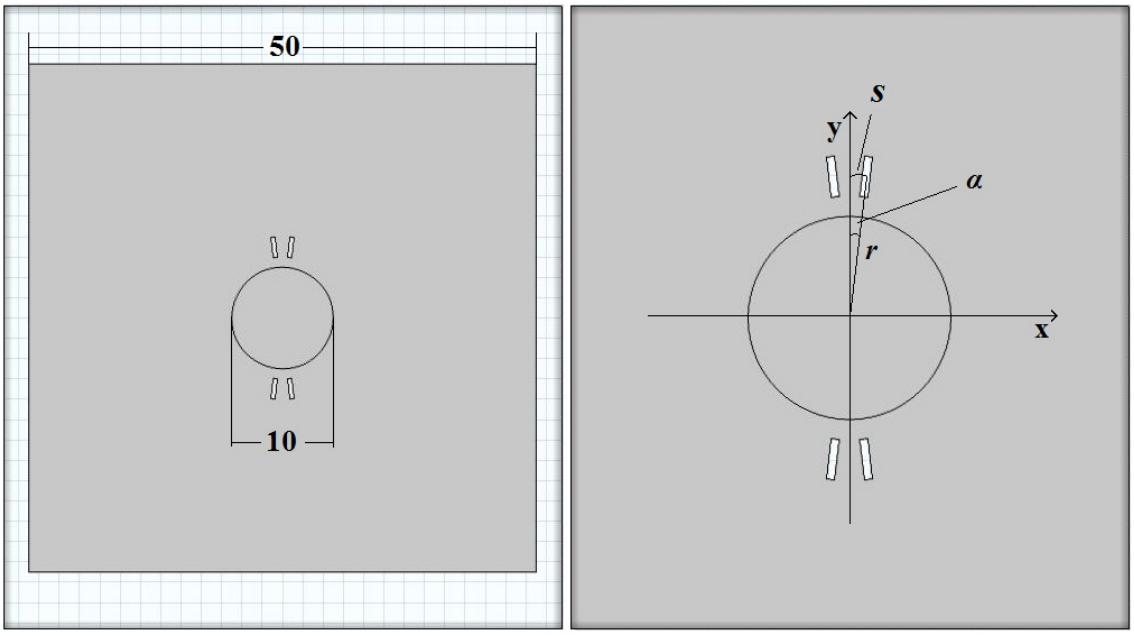

Figure 3.9. *Defined geometry for the EIT models. The dimensions of the model represented in (a) are millimeters. Electrodes are rectangles with length of 2 mm and width of 0.4 mm. The variables used in defining electrode locations at x-y-coordinates are represented in (b): s is the length of the arc between the center of the electrode and y-axis, r is the distance from origin to electrode center and α is the angle between r and y-axis.*

The geometry represented in figure 3.9 is the opposite method. The geometry of the neighboring method is built in the same way, except all four electrodes are next to each other on the same side of the sample. Then the coordinates of the outermost electrodes is calculated according to the inner electrodes knowing that $s = 3 \cdot s_{inner}$. Since r is always

constant in a certain simulation, the angle for outermost electrodes can be calculated according to equation (3.4).

The FEM modeling discretizes the geometry into small elements, an operation called meshing. The size of the elements define the accuracy of the results but also the computational load. Since our model is relatively simple, the mesh size can be defined extremely small without increasing computing time crucially. Meshing is done with different accuracies in different parts of the geometry. The surface of the electrodes and the boundary of the sample are meshed with extremely fine size and the homogenous areas in the sample and aqueous solution with less accuracy. The mesh consists of triangular elements.

3.2.2 Parameters

Parameters needed for modeling are resistivity (or conductivity in COMSOL) and relative permittivity values for each material type used. EIT model consist of three different material types: sample, aqueous solution and electrodes. The electrode material is ignored by subtracting it from the geometry.

Sample resistivity is calculated from the results of viability measurements. The average value of four parallel samples with 0.5 million encapsulated ASCs before heat exposure is applied as is described in chapter 4.1.6. These samples represent best what is the application for EIT in the future. The obtained resistivity is 0.6 Ωm.

During data acquisition, the sample is immersed in an aqueous solution. To model how different resistivity values of the aqueous solution affect the sensitivity field inside the sample, several different values are simulated. As a reference, some known values for water are searched from the literature. The highest resistivity is for purified (distilled and de-ionized) water and reported to be 200 000 Ωm [55]. The lowest resistivity values are for water with large amount of dissolved ions, as for example, sea water with resistivity of 0.2 Ωm. Tap water has a resistivity of 10-50 Ωm, which would be slightly higher than that of our sample. For comparison, saline solution has a resistivity of 5 Ωm. Several values in the region 0.2-200 000 Ωm are modeled. [55], [56]

The permittivity value, as well as resistivity, is dependent on the applied frequency. However, the applied frequency in EIT is less than 1 MHz which is significantly less than what is needed to decrease the relative permittivity of water [6], [57]–[59]. Thus, the permittivity of all tested aqueous solutions and the hydrogel sample is approximated to be 80.

3.2.3 Sensitivity field simulation

The EIT models are implemented using the lead field theory and equation (2.9), presented in chapter 2.7.1 for sensitivity calculation. The current injection techniques

used in EIT simulations are schematized in figure 3.10. The current density field $\boldsymbol{J}_{LI}$ is produced by the current carrying (CC) couple CC1 and CC2, by applying 1 A current from terminal CC1 to ground CC2 (see figure 3.10). The same is done for voltage measurement electrodes PU1 and PU2, which produces a current density field $\boldsymbol{J}_{LE}$. The scalar product of the resulting current density vectors provide the local sensitivity distribution. [38]

In the opposite method, one technique is used, represented in figure 3.10 (a). For the neighboring method, there are three different possibilities as it is illustrated in figure 3.10 (b)-(d). The first technique uses adjacent electrodes for both current injection and voltage measurement. This is called next to -technique. The second technique uses the outer electrodes for current injection and middle electrodes for voltage measurement, and it is called edges technique. The third possibility would be to use every other electrode for current injection and voltage measurement, called every other -technique. The name of the technique indicates which electrodes are CC electrodes: next to -technique uses adjacent electrodes as CC couple, edges technique uses the outermost electrodes and every other -technique the outermost and the third electrode from the left.

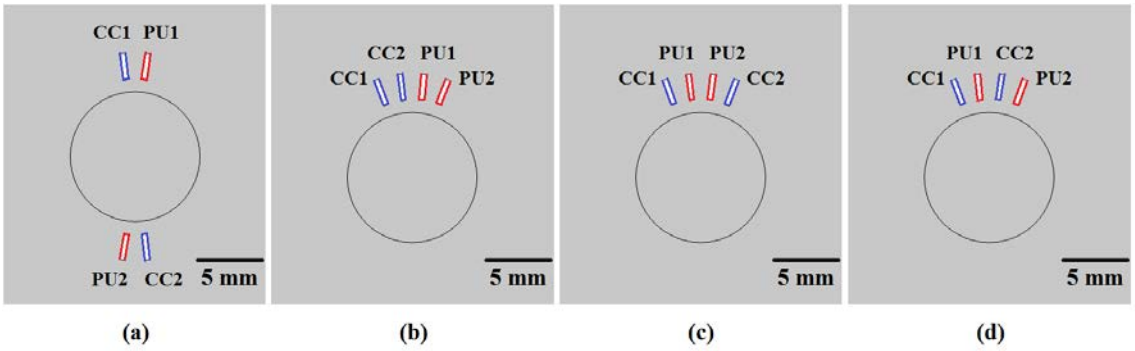

Figure 3.10. *Current injection techniques used in EIT simulations. The opposite method is illustrated in (a) and the neighboring method in (b) - (d). For clarity, they are called: (b) next to -, (c) edges - and (d) every other -techniques. CC1 and CC2 form the current carrying (CC) couple and PU1 and PU2 form the pick-up (PU) couple. Terminals and grounds are highlighted with blue color in CC couple and with red color in PU couple.*

Electrode material is excluded from the EIT model, but the shape and location is modeled. Current is injected and measured from the electrode's outer surface as it is highlighted using blue and red colors in figure 3.10. The back of the electrode is set as electrical insulation. The outer box illustrated in figure 3.9 (a) is also set as electrical insulation domain. The current density fields produced by these techniques are represented in appendix 2.

4. RESULTS

The results of EIS measurements and EIT models are presented in the following subchapters. For EIS measurements, preliminary tests are done to define some parameters as the electrode material. Electrical properties of the blank and bulk materials and phantoms with alumina particles are also studied. Finally, cell gradient and cell viability are studied. Concerning EIT models, the ideal resistivity value for the aqueous solution and the electrode locations are optimized. The former is done for the opposite method only and the latter for both opposite and neighboring methods.

4.1 EIS measurements

EIS results are organized as follows: preliminary measurements, blank and bulk samples, alumina particle samples, cell gradients and cell viability measurements. The main goal of preliminary measurements is to find a suitable electrode material and an optimal sample volume for further measurements. Blank and bulk samples consist of GG hydrogel or cell culture medium or the mixture of these. These are the basic components for the further samples, providing a good reference for cell studies. The goal of cell gradient measurement is to find out if cells have an effect on impedance or not and how much is the cell concentration needed for that. According to cell gradient measurements a suitable cell concentration is chosen and used in cell viability measurements. In the last subchapter, it is determined if cell viability can be distinguished by EIS in GG hydrogel scaffold. All graphs representing the measured impedance spectrums are illustrated as **Bode plots** (see chapter 2.4): the impedance magnitude as a function of frequency on top and the phase as a function of frequency below. Resistivity values are calculated from a purely resistive frequency point.

4.1.1 Preliminary measurements

The first EIS measurements are done using Ag-AgCl (Science Products GmbH, E255B) electrodes of 0.4 mm in diameter and GG hydrogel in small FEP tubes (diameter 2 mm). However, it is noticed that these types of electrodes produced a considerable amount of bubbles when in direct contact with GG-0.6SPM hydrogel. This is the case even without electrical current. According to Jenny Parraga [60], this is most probably caused by a redox reaction between polysaccharides of the hydrogel and the silver in the electrode.

In order to find a material that is stable with GG hydrogel, platinum and gold are tested. Literature review is also done in order to find studies with same type of materials, as

was mentioned earlier. Pt-electrodes are tested with and without electrical current. Few bubbles are readily formed independent of the electrical current.

Another test is performed because some bubbles are produced in some experiments and in some not. A material that should not produce any chemical reaction with the GG hydrogel is tested. A piece of the FEP tube is cut to be same size and shape as the Pt-electrode, cleaned with ethanol and set slowly into the gel. This experiment is done again with tube immersed in distilled water. Even still, many bubbles are formed around the sharp edges and on the tip of the plastic stick during several hours at room temperature. The conclusion is that bubbles can be formed in GG hydrogel by some other mechanism in addition to redox reaction with silver. Because platinum does not cause more bubbles than the FEP material, measurements are carried on using Pt-electrodes. Furthermore, in the measurements it is always avoided unnecessary physical disturbances of the GG hydrogel, as much as possible.

To find the appropriate sample volume, three different volumes of blank GG-1.1SPM hydrogels are measured: 1 ml, 1.5 ml and 2 ml, one sample of each. The results are represented in figure 4.1.

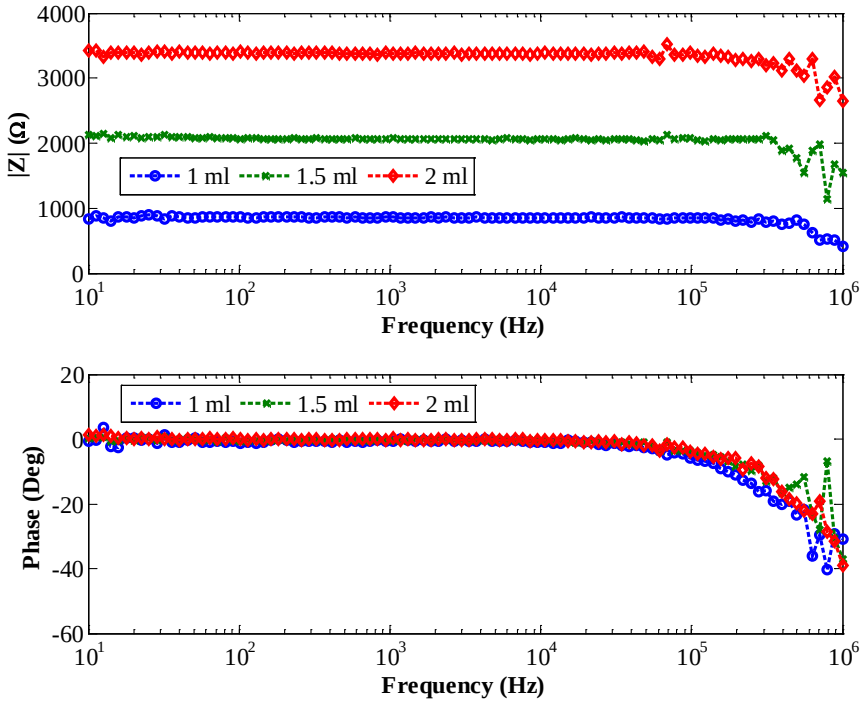

Figure 4.1. *Bode plot of preliminary measurement with three different GG-1.1SPM volumes: 1 ml, 1.5 ml and 2 ml.*

The impedance increases as the sample volume and distance between electrodes increases. For the 1ml sample the measured impedance value is 862 Ω, for the 1.5 ml sample it is 2073 Ω and for 2 ml sample it is 3374 Ω at 1 kHz frequency. The phase is

zero until about 50 kHz and becomes negative above it. Also impedance shows a decrease at frequencies above 100 kHz.

The resistivity values are calculated according to equation (3.2), applying parameter values: R = impedance value at 1 kHz, d = 10 mm and l = the electrode tip distance represented in table 4.1. The error of the resistivity is approximated by equation (3.3), using above-mentioned values and ΔR = 1 % of measured resistance, Δd = 0.1 mm and Δl = 0.1 mm. These results are presented in table 4.1.

Table 4.1. *Resistivity of blank GG-1.1SPM according to three different sample size at 1.0 kHz.*

Sample volume (ml)	**Electrode tip distance *l* (mm)**	**Resistivity $\rho \pm \Delta\rho$ (Ωm)**
1	8.3	8.16 ± 0.34
1.5	14.7	11.08 ± 0.41
2	22.3	11.88 ± 0.41

Resistivity of the smallest sample is about 8 Ωm but for bigger samples it is about 11 Ωm. This suggests that too short electrode distance may cause error in this measurement setup. The estimated maximum errors are only about 4 % of the calculated resistivity. This is mainly because HF2IS system has an accuracy of about 1 %. In EIS measurements it is important that the dimensions of parallel samples are the same. In order to obtain as homogenous electric field as possible but still not wasting the solutions, volumes are optimized to be 1.5 ml for blank and some of the bulk samples. For cell samples 1 ml of hydrogel was chosen to maximize the volume concentration of cells.

4.1.2 Blank and bulk hydrogel samples

Five parallel samples of blank GG-1.1SPM, GG-0.6SPM, cell culture medium and GG-1.1SPM incubated with cell culture medium for 24 hours are measured. The volume of each sample is 1.5 ml which results for all samples in an electrode tip distance of 14.3 mm. Averaging of 8 is used in cell culture medium and bulk measurements, reducing noise in the spectrums. The mean impedance and phase spectrum of each sample type is represented in figure 4.2.

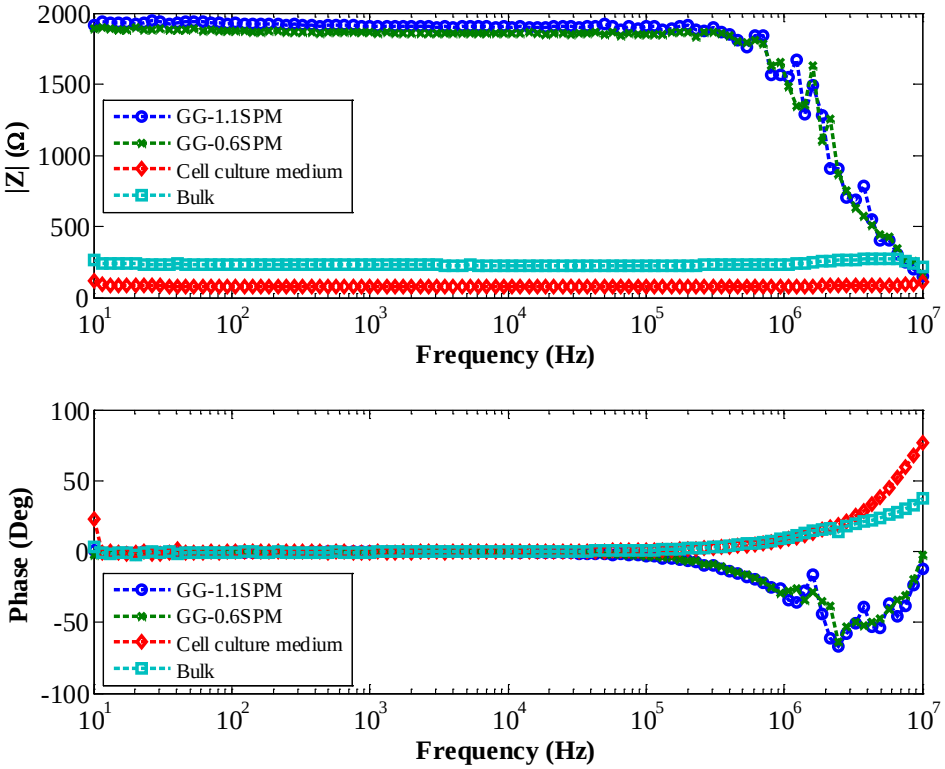

Figure 4.2. *Bode plot of blank and bulk GG hydrogels and cell culture medium. There are two types of blank hydrogels (GG-1.1SPM and GG-06.SPM) with different cross-linker concentrations. Bulk sample is the combination of GG-1.1SPM and cell culture medium. All samples have the same 1.5 ml volume and each curve is a mean value calculated from 5 parallel samples.*

The blank hydrogels are purely resistive (impedance is constant and phase is zero) until about 50 kHz. Above this, a capacitive effect is seen as impedance and phase decreases. Cell culture medium is purely resistive until about 1 MHz, and above this, phase becomes strongly positive and impedance is constant until 10 MHz. The impedance of the bulk sample is constant until 1 MHz and shows a slight increase between 1 MHz and 10 MHz. The phase of bulk is zero until about 1 MHz and becomes positive above this.

The mean values of impedances and resistivities with standard deviations at 50 kHz for all sample types are represented in table 4.2. The mean value of impedance is the same value as is in the figure 4.2 at a frequency of 50 kHz. The resistivity values are calculated for each sample applying following values to the equation (3.2): R = measured impedance value at 50 kHz, d = 10 mm, l = 14.3 mm. The error is now estimated as a standard deviation of the five calculated resistivity values.

Table 4.2. *Mean of impedance and resistivity at 50 kHz for blank hydrogels, cell culture medium and bulk samples. Each mean and standard deviation is calculated from five parallel samples.*

Sample type	**Mean impedance ± std (Ω)**	**Mean resistivity $\rho \pm \Delta\rho$ (Ωm)**
GG-1.1SPM	1930 ± 150	10.58 ± 0.80
GG-0.6SPM	1850 ± 70	10.14 ± 0.37
Cell culture medium	80 ± 3	0.44 ± 0.02
Bulk	230 ± 9	1.25 ± 0.05

The mean impedance of GG-1.1SPM and GG-0.6SPM is about 1.9 kΩ for both. The impedance difference is about 80 Ω and taking into account the standard deviations of 150 Ω and 70 Ω, the difference is not statistically significant. Cell culture medium has considerably smaller impedance than the blank hydrogels: only 80 Ω. The mean impedance of bulk samples is 230 Ω, which is closer to the impedance of cell culture medium than to the impedance of GG-1.1SPM. The resistivity values are in correlation with impedance values: about 10.6-10.1 Ωm for the blank hydrogels, 0.4 Ωm for the cell culture medium and 1.3 Ωm for the bulk.

4.1.3 Hydrogel with alumina particles and medium

Different concentrations of alumina particles are measured. The electrode tip distance is not constant. However, the resistivity values can be compared between different particle concentrations. An example of the frequency spectrum obtained is represented in figure 4.3. Since alumina is known to be purely resistive, the frequency spectrums have similar shape as bulk samples in figure 4.2.

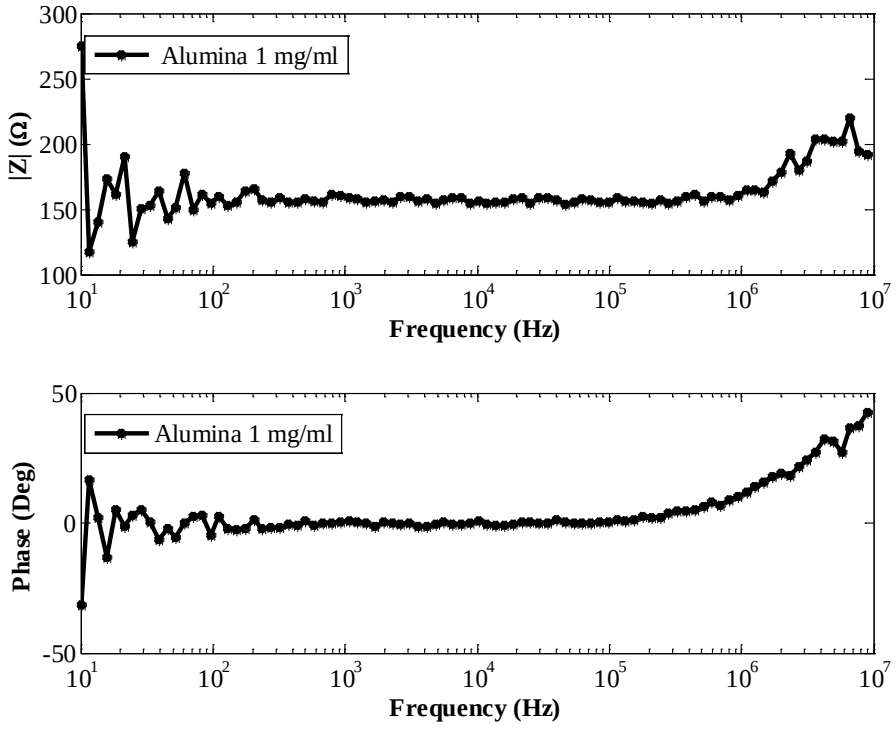

Figure 4.3*. Bode plot of 1 mg/ml of alumina particles in GG-0.6SPM, incubated in cell culture medium for 22 hours.*

The resistivity values are calculated according to equation (3.2), applying values: R = measured impedance value at 50 kHz, d = 10 mm and l = the electrode tip distance represented in table 4.3. The error of the resistivity is approximated by equation (3.3), using above-mentioned values and ΔR = 1 % of the measured resistance, Δd = 0.1 mm and Δl = 0.1 mm. These results are represented according to the alumina particle concentration in table 4.3.

Table 4.3 *Resistivity of different concentrations of alumina particles encapsulated in GG-0.6SPM and incubated in cell culture medium. Resistivities are calculated at purely resistive frequency of 50 kHz.*

Electrode distance *l* (mm)	**Particle mass concentration (mg/ml)**	**Resistivity $\rho \pm \Delta\rho$ (Ωm)**
14.4	0	1.29 ± 0.05
13.5	0.5	1.10 ± 0.04
12.7	1	0.96 ± 0.04
12.3	2	0.96 ± 0.04
11.3	3	1.04 ± 0.04
12.4	4	0.98 ± 0.04

Resistivity is about 1.3 Ωm for the bulk sample, 1.1 Ωm for the smallest particle concentration and 1 Ωm for the other concentrations. Thus, resistivity decreases if there are alumina particles in the hydrogel.

Theoretical resistivity of the suspension according to the volume fraction of alumina particles can be calculated using equations (2.5) and (2.6). First, the volume fraction of each sample in percent is calculated using equation (2.7). Alumina particles can be assumed to be additive in the solution, thus their volume can be subtracted from the final volume ($V_{solution} = V_{final} - V_{spheres}$). Particle volume ($V_{spheres}$) of each sample is obtained by the mass of the particles in each sample (mass concentration in table 4.4 multiplied by 50 µl) and the known density of 750 kg/m^3. The final volume is as follows: $V_{final} = h \cdot \pi(d/2)^2$, where $h = l + 4mm$ and d = 10 mm. The volume fractions are presented in table 4.4.

Table 4.4. Mass concentration and volume fraction of alumina particles.

Particle mass concentration (mg/ml)	**Volume fraction Φ (%)**
0.5	0.002
1	0.005
2	0.01
3	0.02
4	0.02

All volume concentrations are clearly less than one percent. Applying these values together with σ_1 = 1/1.29 S/m for the suspending (resistivity of bulk in table 4.3) and σ_2 = 1/10^{12} S/m for the suspended spheres (alumina), theoretical results are simulated. For theoretical results, a volume fraction range from 0 % to 0.04 % is used and one hundred data points are evaluated. They are plotted together with the resistivity values in table 4.3 and corresponding volume fraction values in table 4.4. These results are illustrated in figure 4.4.

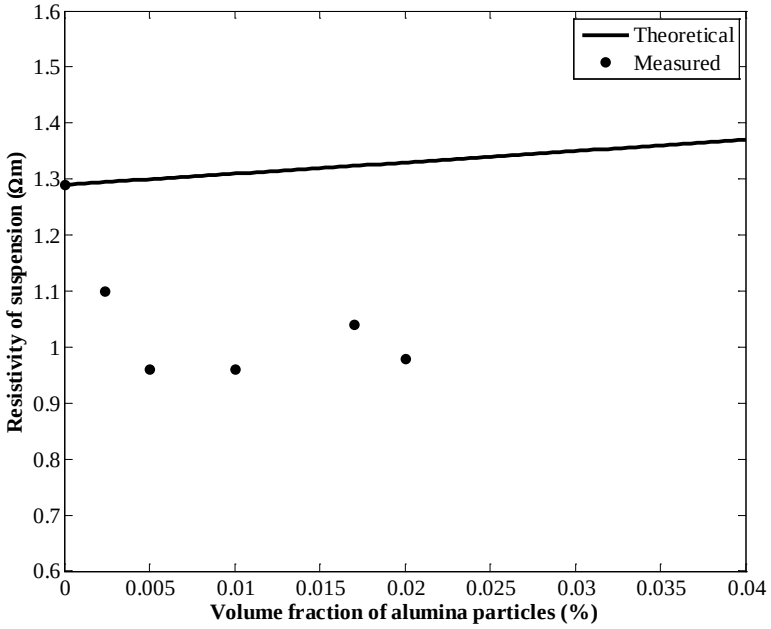

Figure 4.4. *Resistivity of alumina particle suspension as a function of volume fraction. The dots in the figure represent the values obtained according to measurements and the solid line is based on equation (2.5).*

Theoretically, the resistivity of suspension with highly resistive particles increases as the particle concentration increases. However, the resistivity according to the measurements decreases if there is alumina particles present. The measured and theoretical values are the same at zero concentration because σ_1 is based on the measured value and according to equation (2.5): $\sigma = \sigma_1$, when $\Phi = 0$.

4.1.4 Preliminary cell sample measurements

The effect of cells in GG hydrogel is first measured from samples with approximately 375 000 adipose stem cells (single cells and clusters) encapsulated in 1ml of GG-0.6SPM and 1ml of cell culture medium. EIS results are illustrated in separate images since the electrode distance is not constant. They are presented in figure 4.5.

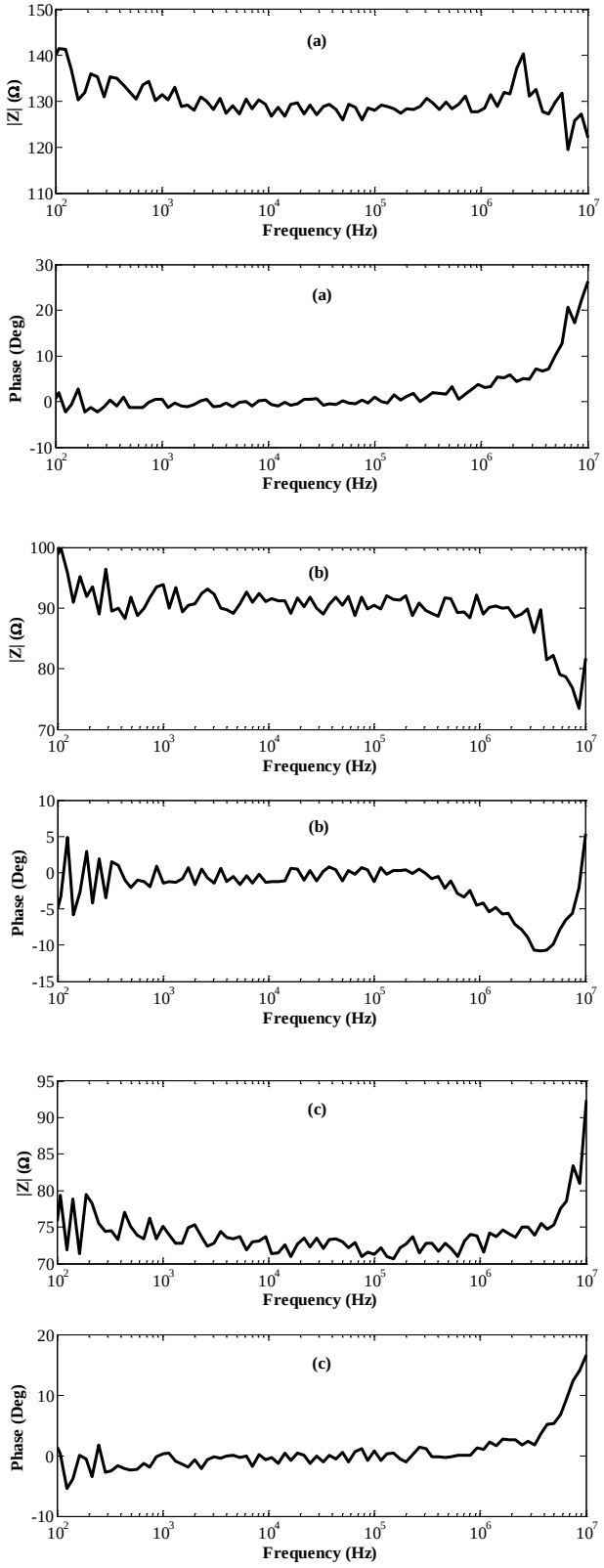

Figure 4.5. *Bode plots of three samples with 375 000 adipose stem cells in GG-0.6SPM and cell culture medium. Distance between electrodes is: (a) l = 10.6 mm, (b) l = 9.1 mm and (c) l = 8.6 mm*

The phase is close to zero until 1 MHz in samples (a) and (c) and above 1 MHz it starts to increase. The impedance of sample (a) is close to 130 Ω until at 1 MHz it slightly increases and then decreases. Sample (b) has a zero phase until 100 kHz, after which it becomes negative. Furthermore, the impedance of the sample (b) is around 90 Ω until above 1 MHz, it shows a slight drop, indicating a capacitive effect. The impedance of sample (c) is about 75 Ω, until at high frequencies increases. Because a weak capacitive effect is detected only in one of the three samples, new measurements with higher cell concentration are conducted.

4.1.5 Cell gradient measurements

For the cell gradient measurements, samples with single cells in 1 ml of hydrogel were prepared. Three different cell quantities are used: 0.1, 1 and 2 million cells and one bulk sample is used as a control. A bright field optical microscopy (OM) image of one sample containing 1 million of ASCs is presented in figure 4.6. The OM image was taken after the EIS measurements. Electrode tip distance *l* is 8.2 mm in all samples.

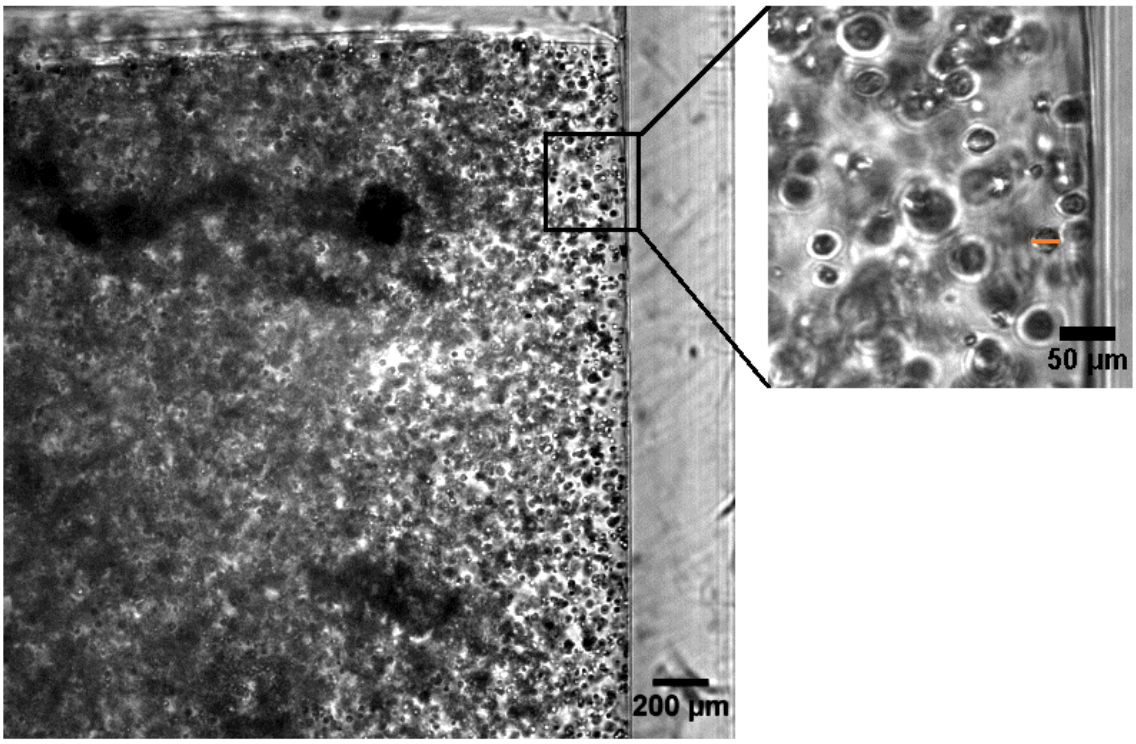

Figure 4.6. *Bright field optical microscope image of a sample with 1 million cells in 1 ml of hydrogel. The cell with an orange bar has 25 µm of diameter.*

The size of one cell can be estimated since it is known that, if 5 x objective lens is being used, 392 pixels in the bright field OM image corresponds to 500 µm in the sample. A cell that is in focus is chosen to be measured as is shown in figure 4.6. The obtained diameter is 25 µm for this certain cell, which is marked with the orange bar. It can be seen from the OM image that the cells have very different sizes.

There are two parallel samples containing 1 million cells but otherwise there is just one sample of each quantity. The impedance and phase spectrums of different cell amounts and the bulk sample are represented in figure 4.7.

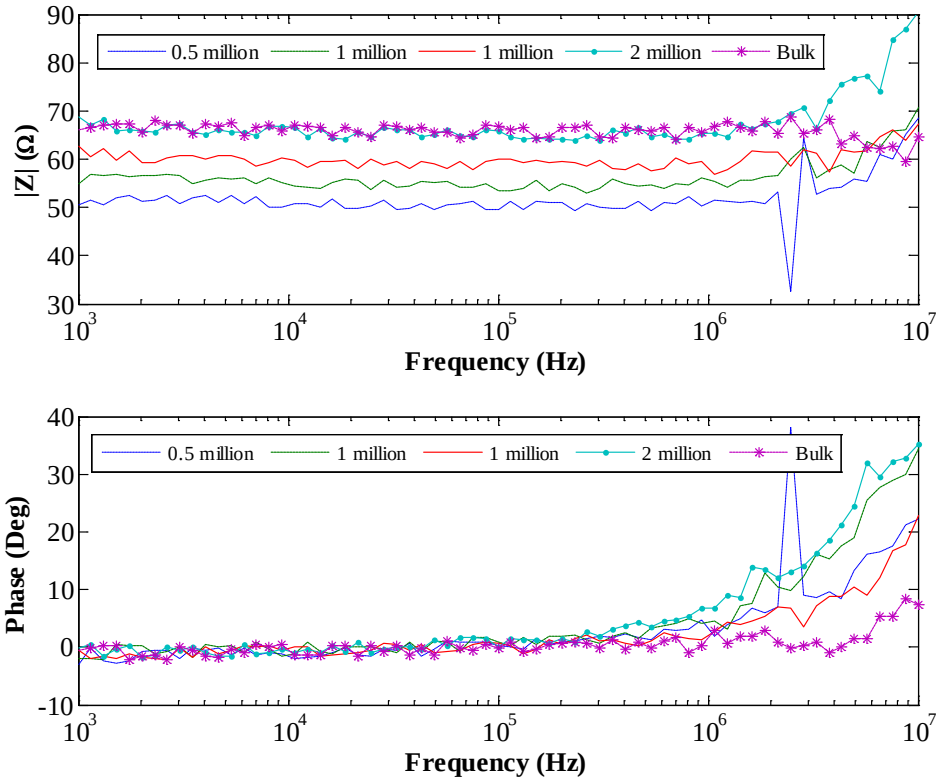

Figure 4.7. *Bode plot of samples with different amounts of cells, GG-1.1SPM and cell culture medium (blue, green, red and light blue lines) and a bulk sample (control, purple line).*

The impedance value is lowest for the smallest amount of cells and it increases towards bulk sample as cell amount increases. No decrease in impedance or negative phase is seen at high frequencies (above 100 kHz), as would have been expected. The phase is zero or slightly negative for all samples until about 100 kHz, when it starts to increase.

The resistivity values for cell gradients are calculated according to equation (3.2), applying values: R = impedance value at 50 kHz (from table 4.5), d = 10 mm and l = 8.2 mm. The error of the resistivity is approximated by equation (3.3), using above-mentioned values and ΔR = 1 % of the measured resistance, Δd = 0.1 mm and Δl = 0.1 mm. These results are represented according to the cell amount in table 4.5.

Table 4.5. *Impedance and resistivity of cell gradient samples at 50 kHz.*

Cell amount (million)	**Impedance $Z \pm \Delta Z$ (Ω)**	**Resistivity $\rho \pm \Delta\rho$ (Ωm)**
0	65.5 ± 0.7	0.63 ± 0.03
0.5	49.5 ± 0.5	0.47 ±0.02
1, no. 1	55.0 ± 0.6	0.53 ± 0.02
1, no. 2	59.0 ± 0.6	0.57 ± 0.02
2	65.0 ± 0.7	0.62 ± 0.03

The highest impedance values are for the bulk sample (65.5 Ω) and the sample with 2 million cells (65 Ω). They have a resistivities of 0.63 Ωm and 0.62 Ωm respectively. The sample with 1 million cells no. 2, has an impedance of 59 Ω and resistivity of 0.57 Ωm, which is almost the same as for two million cells. The samples with 1 million cells no. 1 and 0.5 million cells have the lowest impedance values (55 Ω and 49.5 Ω respectively) and they produce a resistivity of about 0.5 Ωm.

The volume fraction can be calculated for each cell amount N using equation (2.7). According to the measurement from the OM image, cells are approximated to be spheres with radius of $r_{spheres}$ = 25 µm. The volume occupied by the cells is $V_{spheres} = N \cdot (4/3) \cdot \pi \cdot r_{spheres}^3$. The volume of the solution becomes $V_{solution} = V_{final} - V_{spheres}$, where $V_{final} = h \cdot \pi (d/2)^2$ (now h = 12.2 mm and d = 10 mm). The results of the calculations are represented in table 4.6.

Table 4.6. *Volume fraction of different cell amounts in the final hydrogel-cell-cell culture medium suspension.*

Cell amount (million)	**Volume fraction Φ (%)**
0.5	4
1	7
2	16

From table 4.6 it can be seen that the volume fraction for 0.5 million cells is 4 %, for 1 million cells it is 7 % and for 2 million cells it is 16 %. The theoretical equations (2.4), (2.5) and (2.6) can be applied only for dilute solutions. Since this is not the case according to table 4.6, similar simulations are not performed as was done in chapter (4.1.3).

4.1.6 Cell clusters and cell viability measurements

For the cell clusters and cell viability measurements four parallel cell samples and four parallel bulk samples are measured. ASCs are encapsulated into GG-0.6SPM hydrogel as clusters and single cells. A bright field OM image is captured after viability measurements and it is shown in figure 4.8. One cell cluster, which is in focus, is highlighted by an orange circle. Measurements are done during two days: two cell samples and two bulk samples are measured on the first day and two cell samples and two bulk samples on the following day.

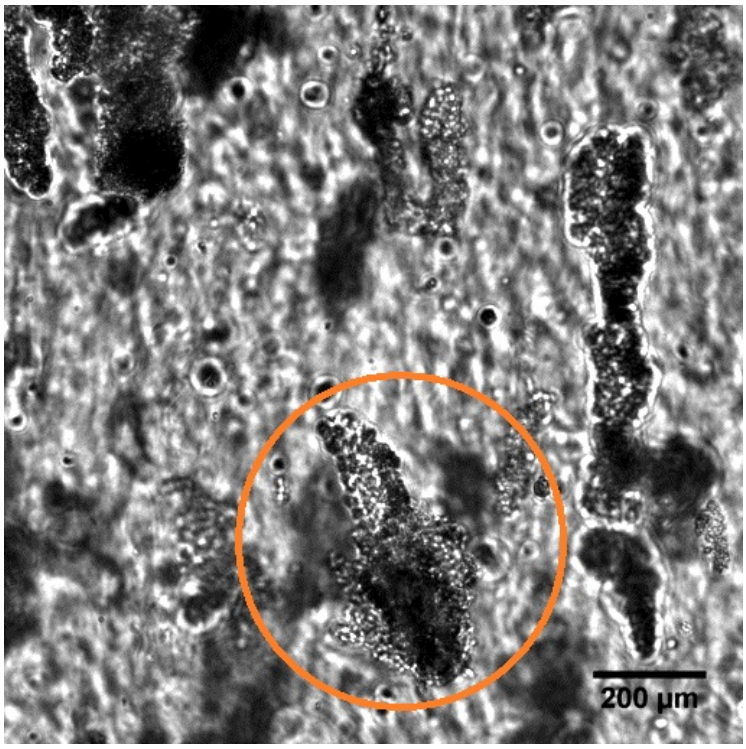

Figure 4.8*. Bright field optical microscopy image of cell clusters in GG-0.6SPM after heat exposure. One cell cluster that is in focus is highlighted with orange circle.*

The EIS measurements of cell samples and bulk samples before and after heat exposure are represented in figure 4.9. Each curve represents the average spectrums of 4 parallel samples. Measurements are done in living cells before heat exposure, dead cells after heat exposure, bulk samples before heat exposure and bulk samples after heat exposure. Averaging of 8 is used in all measurements. The original measurement data is represented in appendix 1.

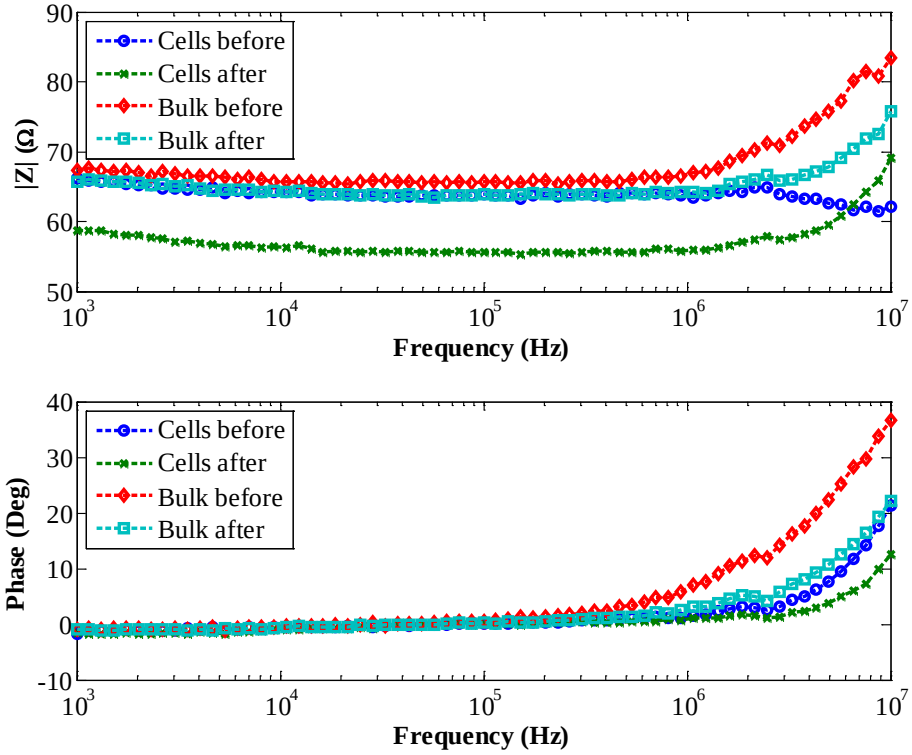

Figure 4.9. *Bode plot of living cells before heat exposure (blue line), cells after heat exposure (green line), bulk samples before heat exposure (red line) and bulk samples after heat exposure (light blue line). Each curve is an averaged result of 4 parallel samples.*

As it can be seen in figure 4.9, the only sample type with a drop in impedance at frequency above 1 MHz is the one with living cells. Other sample types have rather constant impedance until 1 MHz, after which it increases. The mean phase is close to zero for all sample types until 100 kHz or 1 MHz, after which it increases. Another result, which can be seen in figure 4.9 is that the impedance has clearly decreased during the heat exposure in the cell samples. Slight decrease in impedance has also occurred in the bulk samples during the heat exposure. In order to assess if these changes are statistically significant, the mean impedances and the standard deviations at frequency of 50 kHz are calculated from the original results (see Appendix 1). The significance of the impedance change before and after heat exposure is estimated by statistical t-test (MATLAB function *ttest2*) for the cell samples and the bulk samples. These results are represented in table 4.7.

Table 4.7. *Mean impedance at 50 kHz before and after exposure to 43 °C for 2 hours. The significance of impedance change is estimated using statistical t-test.*

		Mean impedance ± std (Ω)	**p-value t-test**
Cells n = 4	Before heat	63.0 ± 3.3	0.0080
	After heat	54.5 ± 2.9	
Bulk n = 4	Before heat	65.1 ± 0.5	0.1921
	After heat	62.1 ± 4.0	

According to the t-test, the change in impedance of the cell samples is statistically significant at 5 % significance level. For bulk samples the null hypothesis cannot be rejected at 5 % level, meaning that the difference in impedances is not statistically significant. The change of mean impedance in cell samples is 63.0 Ω - 54.5 Ω = 8.5 Ω, which means a 13 % percent decrease at 50 kHz.

These measurements have the most amount of parallel cell samples, when compared with the measurements made in previous sub-chapters. Thus, the resistivity value to be used as a parameter in the EIT models is calculated from the mean impedance of living cells. The parameter values applied to equations (3.2) and (3.3) are: R = 63 Ω, ΔR = 0.63 Ω, l = 8.2 mm, Δl = 0.1 mm, d = 10.0 mm, Δd = 0.1 mm. **The obtained resistivity is 0.6 ± 0.03 Ωm.**

4.2 EIT simulations

The neighboring and the opposite methods described in subchapter 3.2.3 are chosen for EIT simulations. In the first study, the resistivity of the aqueous solution is varied and sample resistivity is kept constant. The optimal result of this is then used for the other simulations. The second part is about optimizing the measurement technique in the neighboring method, since there are three possibilities. The most promising one is chosen for to be used in the third part. The third part is about finding the optimal location for electrodes. The first part is done only for the opposite method, second for the neighboring and the third for both methods.

The results are compared numerically using the values obtained in the center of the sample and the most important results are also presented visually. Unless stated otherwise, both the distance between the sample and the electrode tips and the distance between the electrode tips is 1 mm. All images represent sensitivity field with units of $1/m^4$. The data range is from -40 000 $1/m^4$ to 40 000 $1/m^4$ in all simulations of the opposite method and from -20 000 $1/m^4$ to 20 000 $1/m^4$ in all simulations of the neighboring method.

4.2.1 Resistivity optimization

If the aqueous solution around the sample has lower resistivity than the sample, it is likely that most of the electrical current would flow in the aqueous solution and no information of the sample would be measured. On the other hand, if the aqueous solution is highly resistive the voltage drop can be significant in the solution. Several resistivity values in the range of 0.2 Ωm to 200 000 Ωm for the aqueous solution are simulated. The results obtained are summarized in table 4.8 and plotted in figure 4.10.

Table 4.8 *Sensitivity in the center of the sample in the opposite method for different resistivities of the aqueous solution.*

Aqueous solution resistivity (Ωm)	**Sensitivity in the center ($1/m^4$)**
200 000	9300
10 000	9300
30	8900
15	8600
10	8300
5	7400
3	6500
1	3700
0.8	3100
0.6	2400
0.4	1500
0.2	610

The sensitivity shows a knee around 10 Ωm, which is highlighted with a circle in figure 4.10. Above the knee, the sensitivity increases only slightly, even if the aqueous solution resistivity increases significantly. The sensitivity decreases dramatically as aqueous solution resistivity decreases below 10 Ωm.

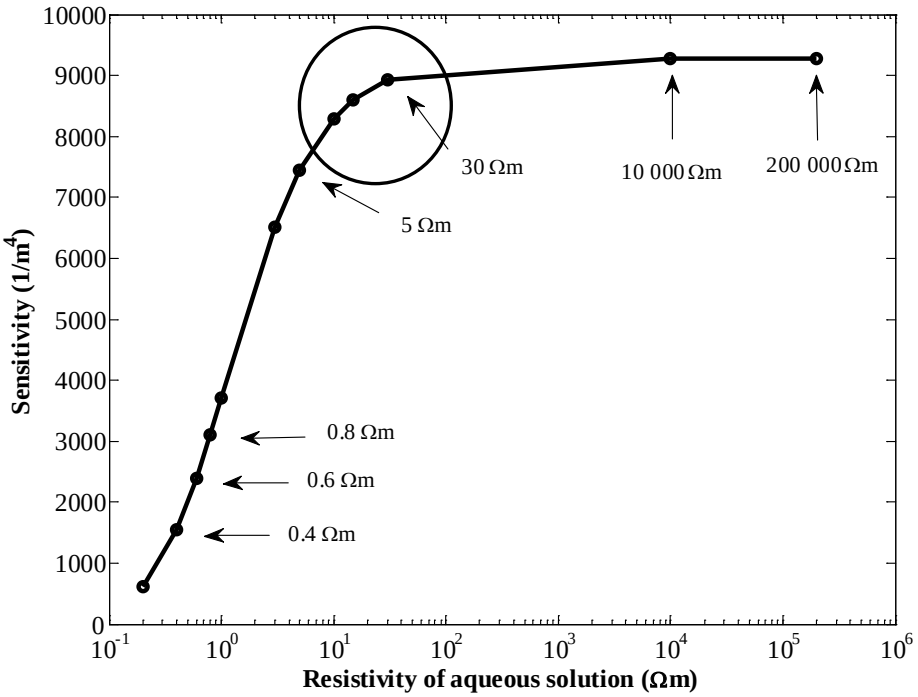

Figure 4.10. *Sensitivity in the center of the sample as a function of aqueous solution resistivity obtained with the opposite method model. The circle indicates the optimal values for the aqueous solution resistivity if sample resistivity is 0.6* Ω*m.*

The variation of the sensitivity in the sample with the aqueous solution resistivity is represented in figure 4.11. Four simulations are represented in the figure with aqueous solution resistivity of 200 000 Ωm, 30 Ωm, 5 Ωm and 0.3 Ωm. The sensitivity is positive (yellow and red colors) or near zero (green color) but never negative (blue color) inside the sample. Negative regions only occur between the electrodes.

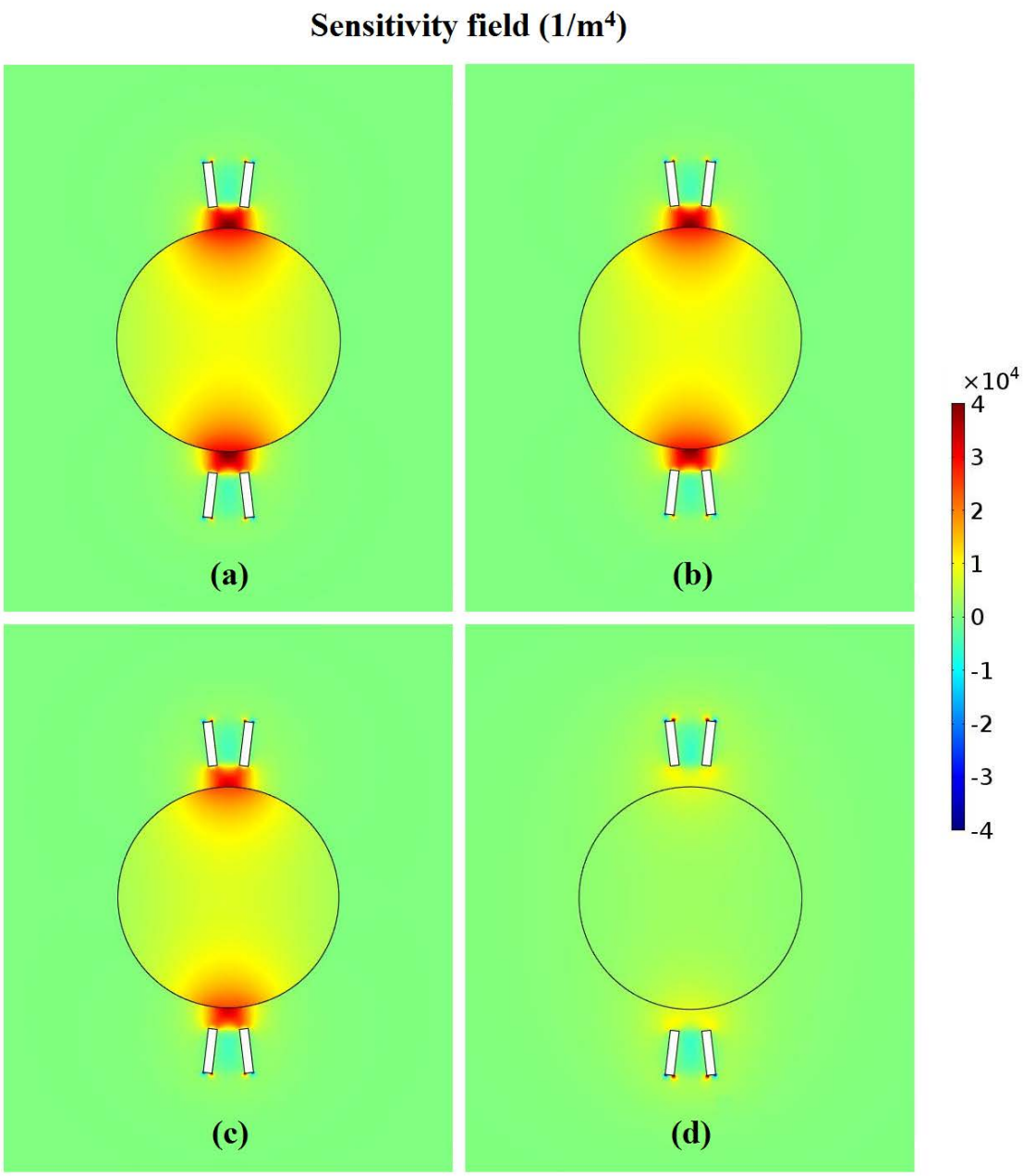

Figure 4.11. *Sensitivity field for different aqueous solution resistivities in 1 cm diameter sample using the opposite method. The aqueous solution resistivities are: (a) 200 000 Ωm, (b) 30 Ωm, (c) 5 Ωm and (d) 0.6 Ωm.*

Figures 4.11 (a), (b) and (c) are visually close to each other. This is in accordance with the sensitivity values that are between 7400 $1/m^4$ and 9300 $1/m^4$ for resistivities from 5 Ωm to 200 000 Ωm. However, the sensitivity drops to 2400 $1/m^4$ when the aqueous solution has the same resistivity as the sample. In accordance with the results, 30 Ωm is chosen for the aqueous solution in further simulations.

4.2.2 Current injection techniques in the neighboring method

There are three different options for the current injection technique, described in chapter 3.2.3: next to -technique, edges -technique and every other -technique. These techniques are modeled and the optimal of these is then chosen to be used in further simulations. The simulation results are shown in table 4.9 and in figure 4.12. The current density fields of these techniques, as well as for the opposite method, are illustrated in appendix 2.

Table 4.9. *Sensitivity in the center of the sample for different current injection techniques for the neighboring method.*

Current injection technique	**Sensitivity in the center ($1/m^4$)**
Next to	60
Edges	300
Every other	600

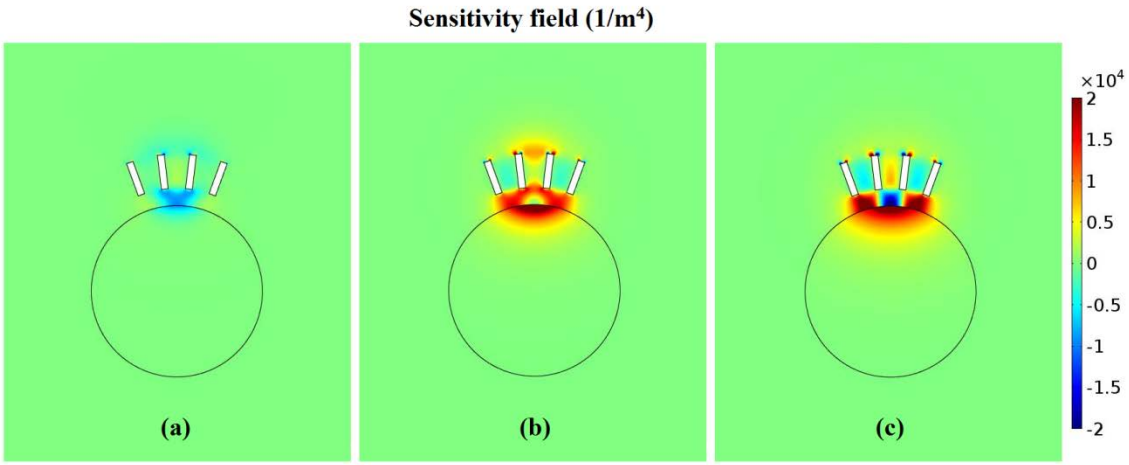

Figure 4.12. *Sensitivity field for different measurement techniques in the neighboring method: (a) next to, (b) edges and (c) every other. Sample has a diameter of 1 cm.*

The sensitivity in the center of the sample is highest in the every other -technique with a value of 600 $1/m^4$. The edges -technique produces a sensitivity of 300 $1/m^4$ and the next to -technique only of 60 $1/m^4$ in the center of the sample. Both next to- and every other -techniques have a negative sensitivity (blue color in images) between the middle electrodes. The every other -technique is chosen for the electrode optimization simulations because it produces the strongest and largest sensitivity field inside the sample.

4.2.3 Electrode location optimization in the opposite method

First, the effect of increasing or decreasing the electrode separation from each other is simulated. Then, the distance between the electrodes is kept constant (1mm) and the distance between sample and electrode tips is studied. The resistivities are constant: for sample it is 0.6 Ωm and for aqueous solution it is 30 Ωm. The results for the first part are represented in table 4.10 and visualized in figure 4.13.

Table 4.10. *Sensitivity in the center of the sample as a function of electrode separation using the opposite method. Distance from the sample is 1 mm.*

Electrode separation (mm)	**Sensitivity in the center ($1/m^4$)**
0.5	9000
1	8900
2	8400
3	7800

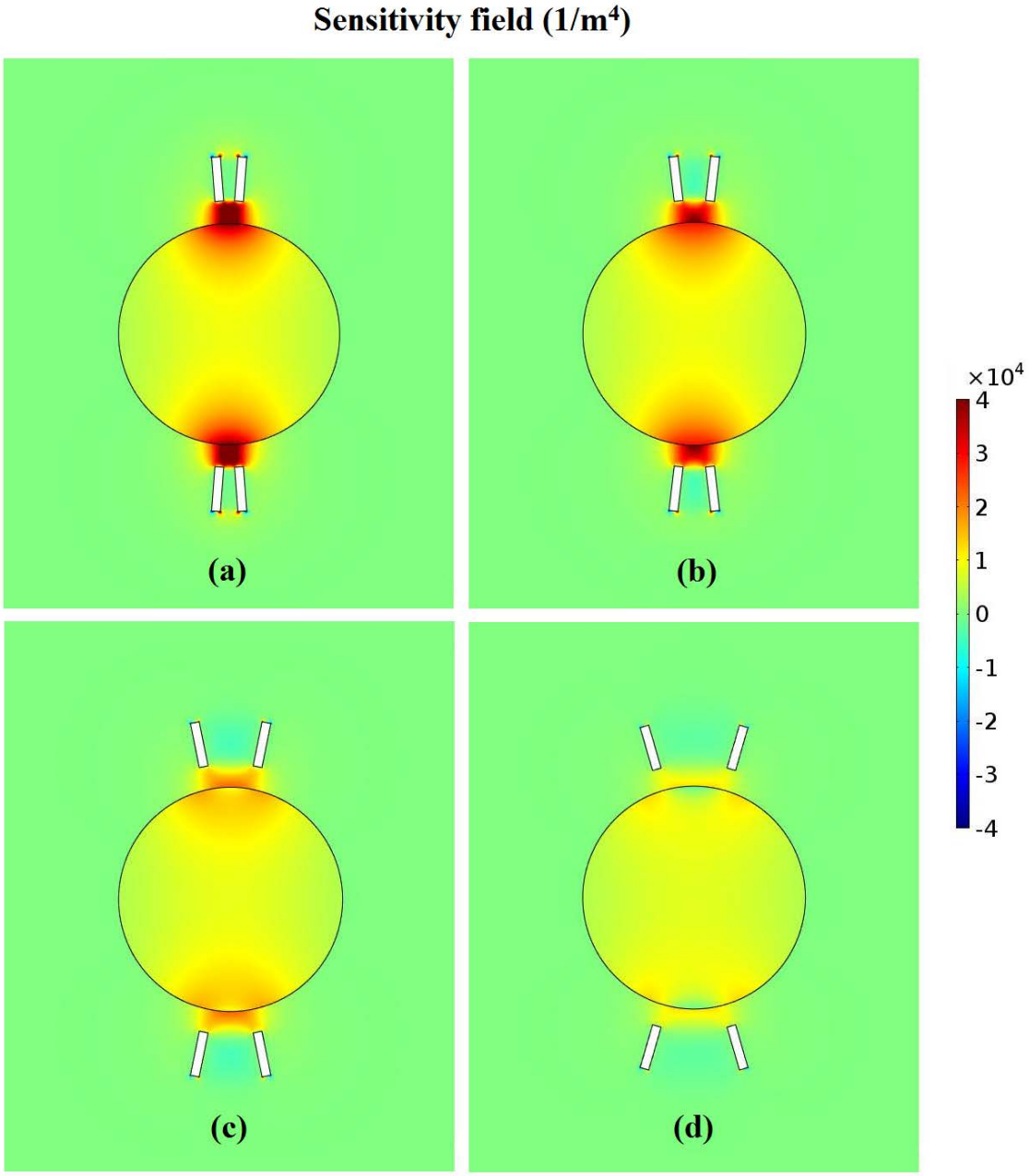

Figure 4.13. *Sensitivity field for different electrode separations from each other using the opposite method. The distance between electrode tips: (a) 0.5 mm, (b) 1 mm, (c) 2 mm and (d) 3 mm. Distance from the sample is 1 mm and sample has a diameter of 1 cm.*

The sensitivity in the center varies from 7800 $1/m^4$ to 9000 $1/m^4$ so that the closer the electrodes are the stronger the sensitivity is inside the sample. A distance of 1 mm is chosen for the further simulations, even though 0.5 mm would produce the highest sensitivity value. This is because, if these type of stick electrodes were used in a practical measurement setup, 0.5 mm separation could cause accidental direct contacts between electrodes. Furthermore, with this separation the capacitive effects between the electrodes are reduced.

In the second study, the electrode distance from the sample is simulated with values of 0.1 mm, 0.5 mm, 1 mm and 2 mm. The results are represented in table 4.11 and visualized in figure 4.14.

Table 4.11. *The sensitivity in the center of the sample according to the electrode tip distance from the sample using the opposite method. The separation between electrode tips is 1 mm.*

Electrode distance from the sample (mm)	**Sensitivity in the center ($1/m^4$)**
0.1	12 900
0.5	10 500
1	8900
2	6900

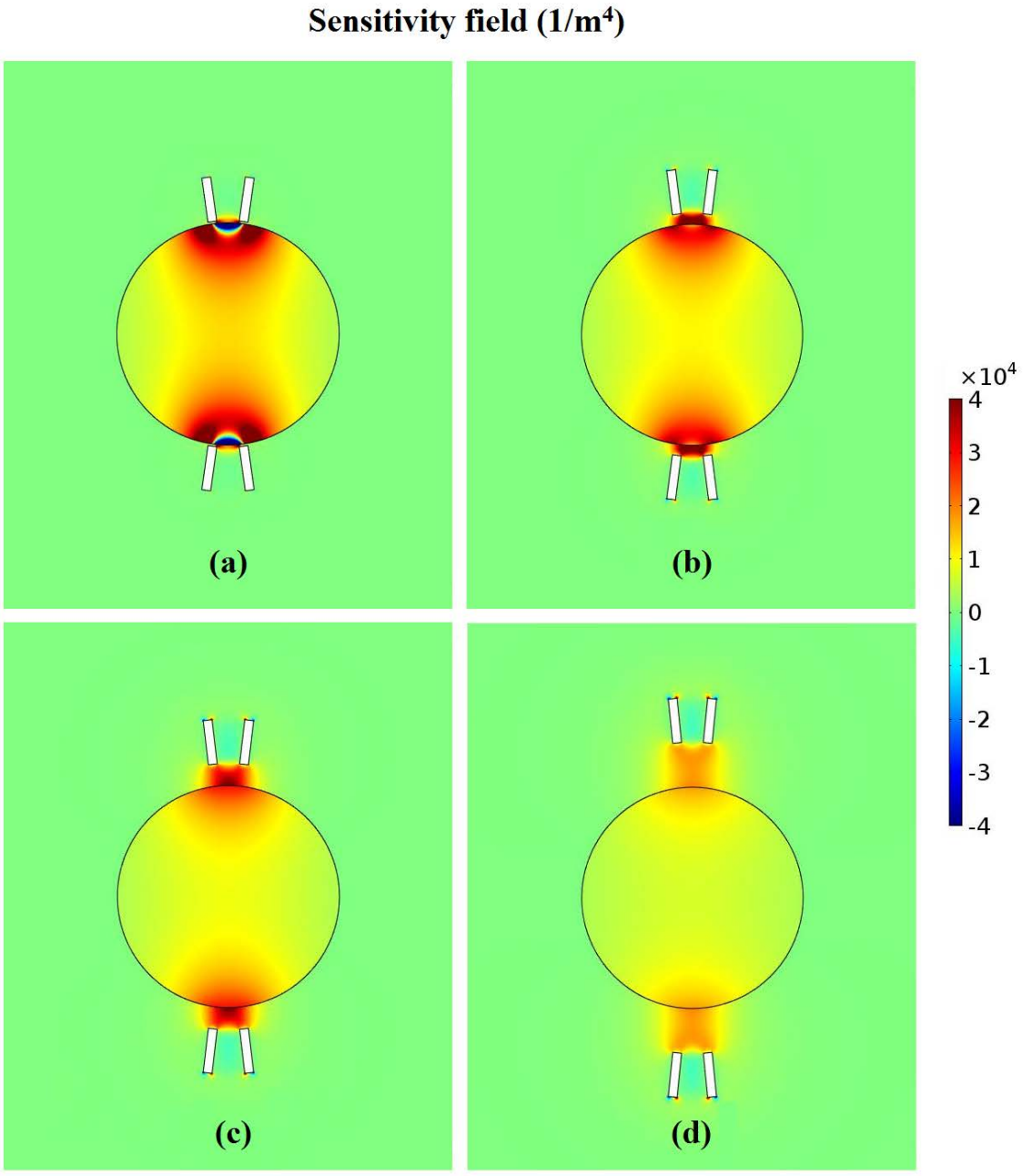

Figure 4.14. *Sensitivity field for different electrode distance from the sample using the opposite method. The distances between electrodes and sample are: (a) 0.1 mm, (b) 0.5 mm, (c) 1 mm and (d) 2 mm. The separation between electrode tips is 1 mm and sample has a diameter of 1 cm.*

The closer the electrodes are to the sample the higher sensitivity is produced in the middle of the sample. In the case where the electrodes are only 0.1 mm away from the sample, the sensitivity is as high as 12 900 $1/m^4$ in the center of the sample. However, there is a negative area between electrodes inside the sample, as it is shown in figure 4.14 (a). Placing the electrodes further away from the sample prevents this negative area, as is shown in figures 4.13 (b)-(d).

4.2.4 Electrode location optimization in neighboring method

Similar steps are done using the neighboring method as was done using the opposite method: first the separation between electrode tips is simulated and then the distance between electrodes and the sample. The resistivities are constant: for sample 0.6 Ωm and aqueous solution 30 Ωm. The measurement technique in the neighboring method is chosen to be every other -technique. Results for the first study are represented in table 4.12 and visualized in figure 4.15.

Table 4.12. *Sensitivity in the center of the sample as a function of the separation between electrode tips using the neighboring method and every other -technique. The distance from the sample is 1 mm.*

Electrode separation (mm)	**Sensitivity in the center ($1/m^4$)**
0.5	300
1	600
2	1300
3	2200

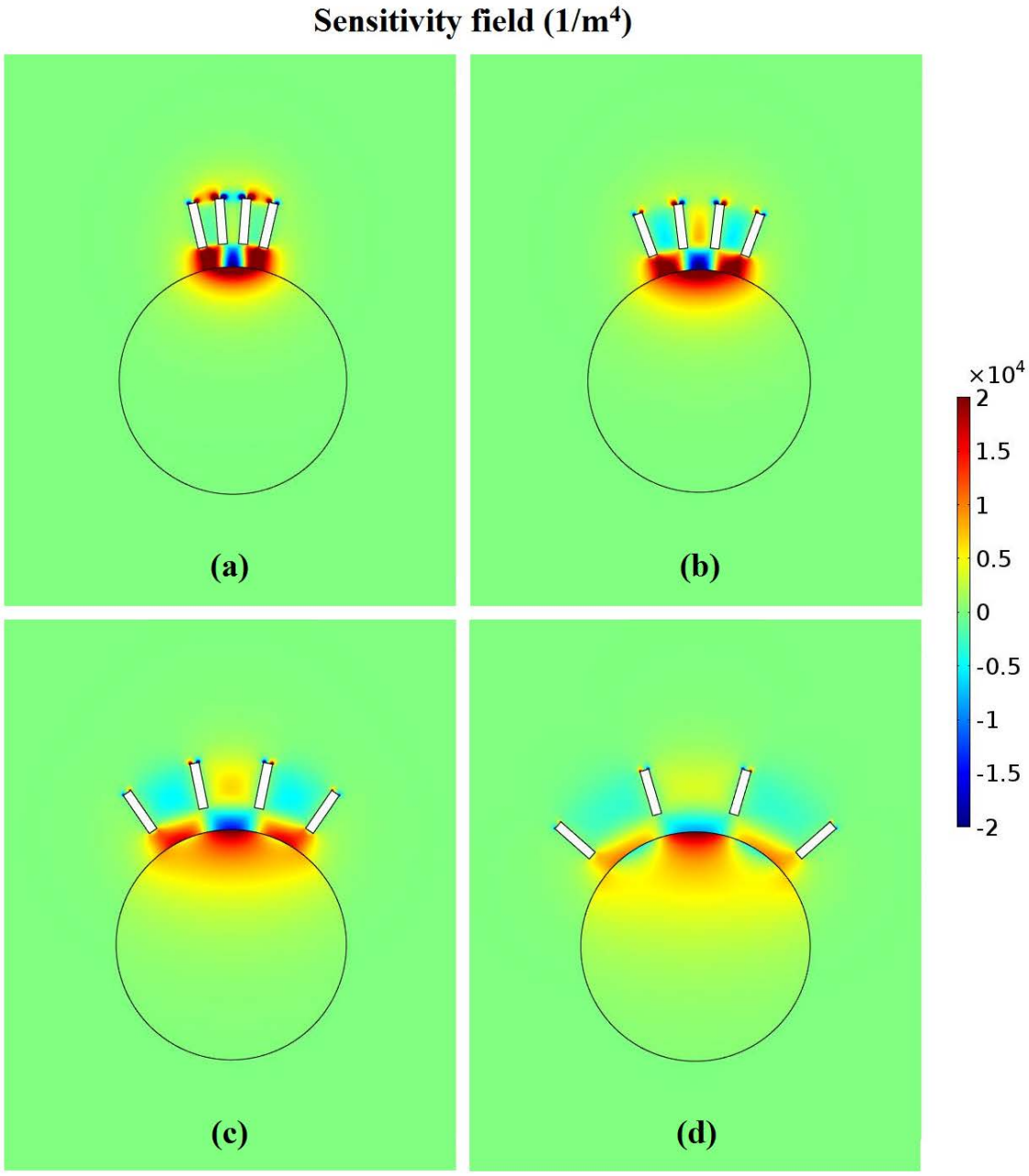

Figure 4.15. *Sensitivity field for different electrode separations using every other - technique in the neighboring method. The separations between electrode tips are: (a) 0.5 mm, (b) 1 mm, (c) 2 mm and (d) 3 mm. Distance between electrodes and the sample is 1 mm and sample has a diameter of 1 cm.*

In the neighboring method, the electrode separation affects crucially on how deep regions are scoped. Increasing the electrode separation enhances the sensitivity in the center of the sample, but also makes the field weaker at the boundaries, as is shown in figure 4.15. There are also negative areas on the edges of the sample if electrode distance is 2 or 3 mm. For the neighboring method, the optimal electrode separation would be 1 mm, thus it is chosen for further simulations.

In the second study, electrode distance from the sample is simulated using the values: 0.1 mm, 0.5 mm, 1 mm and 2 mm. The results are represented in table 4.13 and visualized in figure 4.16.

Table 4.13. *The sensitivity in the center of the sample for different electrode tip distances from the sample using the neighboring method. The distance between electrode tips is 1 mm.*

Electrode distance from the sample (mm)	**Sensitivity in the center ($1/m^4$)**
0.1	1000
0.5	700
1	600
2	300

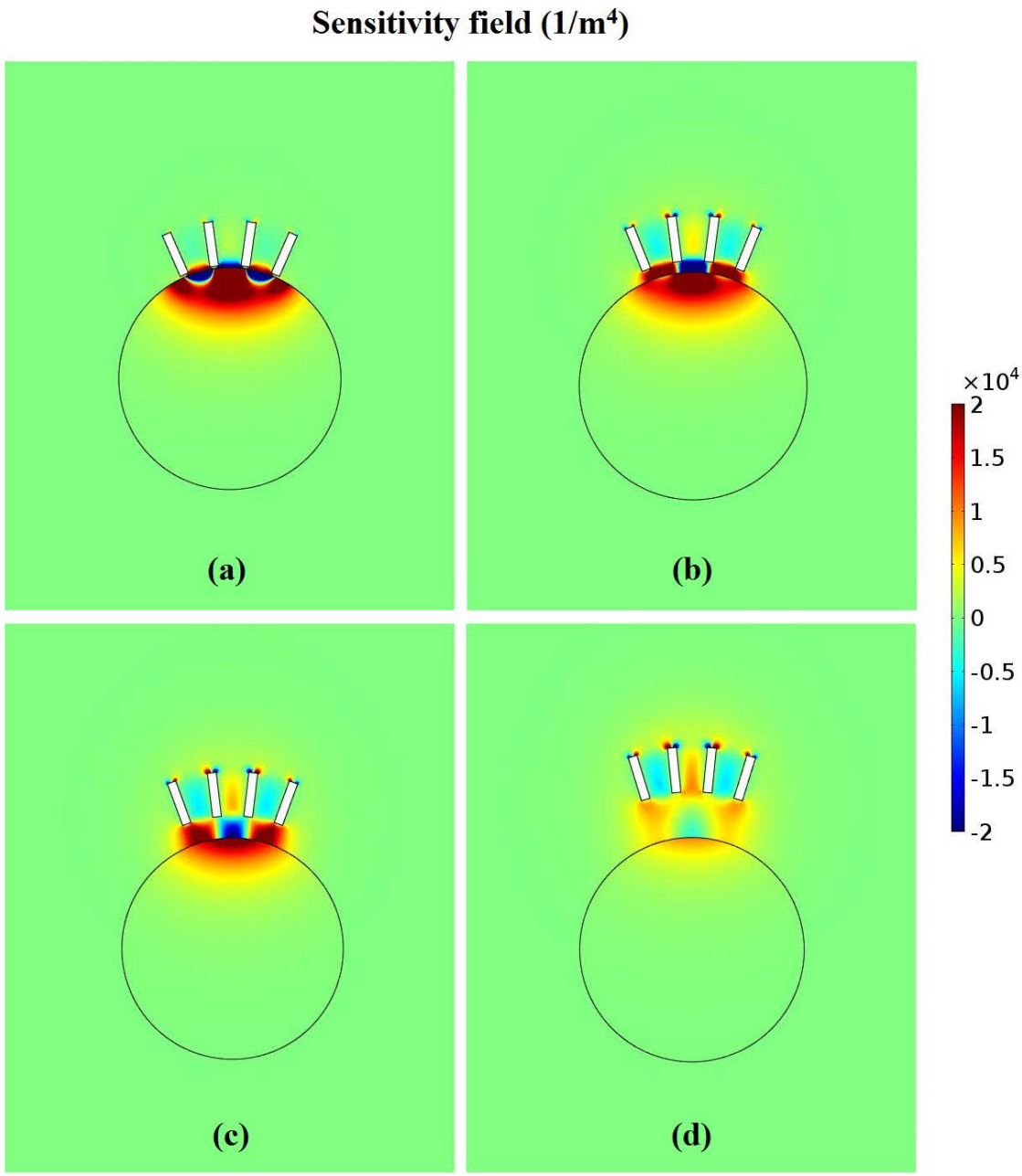

Figure 4.16. *Sensitivity field for different electrode distances from the sample using the neighboring method. The distance between the tip of the electrodes and the sample are: (a) 0.1 mm, (b) 0.5 mm, (c) 1 mm and (d) 2 mm. Electrode tip separation is 1 mm and sample has a diameter of 1 cm.*

Increasing the electrode distance to the sample decreases the sensitivity in the center of the sample. However, placing electrodes very close (0.1 or 0.5 mm) to the sample causes negative region inside the sample. The optimal electrode distance to the sample would be between 0.5 mm - 1 mm when using the neighboring method.

5. DISCUSSION

In this chapter the main results are summarized and analyzed. First, the EIS results and the main error sources are discussed. Then the EIT simulations and their limitations are considered.

5.1 EIS measurements

All EIS measurement results are represented as Bode plots in subchapter 4.1. The Nyquist plot is also introduced in subchapter 2.4, but it is not used in this thesis, since the results are mostly resistive. The data analysis of EIS results is typically based on mathematical model or equivalent circuit fitting, as is mentioned in subchapter 2.4. These methods are not employed for the same reason the Nyquist plot is not used, they would not have provided further information, since the results are mainly resistive.

The EIS results are presented and analysed separately, even though they would have comprised of the same constituents. For example, the bulk in alumina particle measurements is similar to the bulk samples in viability measurements: both are GG-0.6SPM incubated in cell culture medium. However, they are not equivalent because the samples are incubated a different duration at 37 °C before the EIS measurements.

5.1.1 Analysis of the results

From the **preliminary impedance measurements** it can be seen that the Ag-AgCl electrodes cannot be used in contact with GG hydrogel cross-linked with SPM and that 1.5 ml of sample volume would be the optimal volume for EIS measurements using the setup developed in this thesis. The redox reaction between Ag-AgCl electrodes and GG hydrogels led to several tests using different materials in contact with GG hydrogel. It is found that some bubbles are easily formed in the GG hydrogel, especially on the surfaces and edges and that platinum is not inducing bubbles more than the FEP material itself. During further measurements, it is noticed that the higher the temperature and the more time the GG hydrogel is incubated in that temperature, the more air bubbles will be formed. It is also noticed that the bubbles disappear when the samples are in the fridge overnight. A reason for the bubble formation can be as simple as what happens in a glass of water when left to warm to room temperature: the atmospheric gases such as nitrogen and oxygen can dissolve in water (in our case hydrogel) and as the water gets warmer, nitrogen and oxygen slowly come out of the solution forming tiny bubbles at sites with microscopic imperfections on the glass [61].

EIS measurements in **blank samples** proved that GG-1.1SPM and GG-0.6SPM behave purely resistive until about 100 kHz frequency with impedances of approximately 1.9 kΩ in our EIS setup. Above this frequency, the impedance and phase decreases showing that blank hydrogels have capacitive properties. The impedance of the **cell culture medium** DMEM/F-12 and of **bulk** sample (GG-1.1SPM incubated in DMEM/F-12 for 24 hours) are 80 Ω and 230 Ω, respectively. These samples behave as purely resistive material until 1 MHz, and above this the phase increases. The cell culture medium has constant impedance until 10 MHz but bulk samples show a slight increase in impedance above 1 MHz. These measurements show how dramatic effect the cell culture medium has on the measured impedance of hydrogel samples. The bulk impedance is only 12 % of the blank GG-1.1SPM and the capacitive effect disappears. This is probably caused by the high ion content of the cell culture medium and that the porous structure of the hydrogel is filled with the solution.

The encapsulation of **alumina** particles into the bulk sample decreases the resistivity of the sample, although in theory, inserting highly resistive particles into a suspension, should result in the increase of its resistivity. Five different particle concentrations are tested and all samples produce smaller resistivity than the bulk sample. This indicates that the particles may have caused the well conducting cell culture medium to diffuse more efficiently into the hydrogel and thus decreasing the resistivity. The alumina particles used have a diameter of 7 µm on average, causing the volume fraction to be far less than 1 %.

What can be seen from the **preliminary cell samples** is that one sample of three showed some capacitive effects at frequencies above 1 MHz. This implies that the cell concentration may have been too small to be detected by EIS. Thus more cells are encapsulated in the **cell gradient measurements.** The introduction of cells into bulk samples has a similar effect of introducing alumina particles, since the impedance and resistivity decreases. Although, this is the case only when the original ASC amount is 0.5 million or 1 million. If there are 2 million of ASCs, the impedance and resistivity is practically the same as for the bulk sample. This difference can be cause by the cell metabolism. It is possible that 2 million cells have consumed more ions of the well conducting cell culture medium than 0.5 or 1 million cells, causing the resistivity to increase again.

Another result of the cell gradient measurements is that there is no decrease in impedance or negative phase as a sign of the cells capacitive effect in any of the four samples. This is most probably a result of the small cell size and that the cells are encapsulated as single cells, not in clusters. Cells can be compared to plate capacitors, with capacitance directly proportional to the area covered by the plates and inversely proportional to the distance between them. Thus ASCs possess a really small membrane area and the capacitance is very small. To overcome this problem cell clusters are used in the viability measurements.

The **cell clusters and cell viability** measurements answer to two different questions: can the capacitive effect of living cell clusters in the bulk sample be detected and how does the impedance change due to heat exposure. A drop in impedance above 1 MHz frequency is detected from the mean result of living cells. However, the mean phase is positive and does not indicate capacitive effect. This is due to the fact that a clear capacitive effect is measured only in one sample of four parallel samples (see appendix 1). The measurements before and after heat exposure reveals a decrease of 13 % in the impedance in the cell samples and a 5 % decrease in the bulk samples. Impedance decreases in cell samples because dead cells have a ruptured membrane allowing current to pass easily through the cytoplasm.

5.1.2 Error sources and limitations in EIS measurements

Error sources that concern all implemented EIS measurements are: air bubbles, disturbances at high frequencies, as is shown in figure 3.8, and manual placing of electrodes. There is practically in all measurements some amount of bubble formation, but usually limited to 1-4 bubbles on the surface of the tube or holder with diameter of less than 1 mm. If a bubble is formed on the electrode tip before measurements, electrodes are carefully moved further from the bubble. According to test measurements of the reference circuit, the impedance value is reliable until about 4 MHz. Above 1 MHz the phase becomes strongly positive, indicating an inductive coupling from the 116 cm long BNC cables. The manual placing of electrodes can cause small differences on the real electrode distance *l*. However, each measurement is carried out as carefully as possible.

The air bubbles are a problem especially in the viability measurements, since keeping the samples at high temperature for several hours caused the growth of some bubbles to a couple of mm in diameter near electrodes. This effect is not as strong in samples that contain cells when compared to bulk samples. The developed setup is not optimal for measuring the impedance of a liquid because the placing of the holders and electrodes is tricky. As a result, there is one large air bubble in the middle of each cell culture medium sample, which may cause larger impedance values than they really are.

Leaking of parafilm from the lower part of the tube during incubation is a problem concerning the samples that contain cell culture medium on top of the hydrogel. For some samples, a hole was formed in the parafilm that caused some or all of the cell culture medium to flow out of the tube. If this has an effect on impedance or not is not determined yet.

Electrical field is not homogenous in the sample because stick electrodes are used instead of plate electrodes. This can cause uncertainty especially in cell sample measurements due to the small amount of sample volume used. The small volume was chosen in order to maximize the cell concentration in the sample.

Samples with living cells and especially ASCs are highly complex, because of the variance in cell size and cell metabolism. In cell measurements, an assumption is made that cells are alive during the measurements, but this is not verified by any method. However, it can be assumed that at least 90 % of the ASCs are alive. Furthermore, cell response to hyperthermia is expected to vary between cell lines [42], [50]. Thus if these measurements are repeated using different type of cells, it is expected to have different results.

5.2 EIT models

All results obtained in EIT models are based on the equation (2.9). Thus all the images represent the scalar product of the two current density fields. The value of a scalar product depends on the calculated magnitude of the current density vectors in each mesh node, and on the angle between the vectors. The larger the vectors are, the stronger the sensitivity field becomes. However, this is also governed by the cosine of the angle between them. In the case where vectors are parallel, the sensitivity is maximized. If the vectors are antiparallel, the sensitivity is negative. If they are at an angle of 90 °, the sensitivity is zero. A negative sensitivity makes the interpretation of measured data more complicated.

5.2.1 Analysis of EIT simulations

The **resistivity simulations** show that the aqueous solution should have higher resistivity value than the sample. Because the aqueous solution should not be too resistive, the optimal resistivity would be about 30 Ωm in the case that sample resistivity is 0.6 Ωm. Thus aqueous solution with a resistivity of 50 times the sample resistivity provides a good difference between the solution and the sample.

Electrode location optimization in the opposite method shows that if electrodes are close to each other, the current density fields become more parallel, producing a strong positive sensitivity field with values up to 9000 $1/m^4$ in the center of the sample. To avoid possible capacitive effects between electrodes, 1 mm electrode separation is chosen to be optimal. Simulations with different electrode distances from the sample proved that even a difference of 0.4 mm in electrode location can make a big difference in the sensitivity field. If electrode distance is 0.1 mm from the sample, the sensitivity in the center of the sample is as high as 12 900 $1/m^4$ but there is negative regions in the sample between electrodes. If electrode distance is increased to 0.5 mm from the sample, the sensitivity drops to 10 500 $1/m^4$ in the center of the sample, but now the negative region has decreased. Because sensitivity decreases as distance from the sample increases a distance between 0.5 mm - 1 mm would be optimal in the opposite method.

It is known that the probe depth is about the same as the electrode separation for a homogenous sample, if electrodes are placed horizontally, for example on a disc, next to the sample [31], [40]. This is visualized in the **electrode location optimization in the neighboring method**, since placing electrodes further apart increases the sensitivity in the center of the sample. In this case, moving from 0.5 mm to 3 mm separation increases the sensitivity from 300 $1/m^4$ to 2200 $1/m^4$. However, sensitivity at the edges of the sample become weak as sensitivity is increasing in the center. Thus an electrode separation of 1 mm would be optimal for the neighboring method. Simulations of different electrode distances from the sample revealed the same effect as it was seen in the opposite method: placing electrodes very close (0.1 mm distance) to the sample causes a negative sensitivity between electrodes. Going further, decreases the negative area but also causes the sensitivity to drop, thus a compromise needs to be done in the electrode placing. An optimal distance from the sample would be 0.5 mm in the neighboring method.

The opposite and the neighboring methods are very different from each other. Even the highest value in the center of the sample in the neighboring method, is far from the ones obtained by the opposite method. This is expected since current is conducted differently in these methods.

5.2.2 Error sources and limitations in EIT models

Simulations are done by injecting 1 A of DC current through the electrodes which are set to be its terminals. In practice, much smaller AC current will be used. The amplitude of used current is not crucial since it is only a matter of scaling. Shifting to AC studies can reveal capacitance between electrodes. In addition, the EIT models ignore the electrode material and the contact impedances.

In the used models, the back part of the electrodes is set as electrical insulation. This is not the case in practice and some current is lost to surroundings. Sensitivity fields are based on the reciprocity theorem, which assumes the sample to be linear and passive. This might not be the case for living cells. In addition, sensitivity values are taken manually from the center in each simulation. This is why the accuracy of the result is not optimal.

6. CONCLUSIONS

In this thesis, the EIS measurements are performed on 3D samples of hydrogels, hydrogels with encapsulated alumina particles and hydrogels with encapsulated ASCs. The ability of EIS to detect the amount and viability of cells in 3D hydrogel scaffold is studied. In addition, 2D simulations of a new type of EIT setup are performed. In this setup, the electrodes are not in contact with the sample and they are placed at certain areas near the sample, thus not spanning the whole circle. According to the simulations, an optimal resistivity for the aqueous solution between electrodes and the sample is determined and the location of the electrodes is optimized.

EIS results were surprising since capacitive effect was present only in two individual cell samples. Both of these samples contained cells in clusters. The lack of capacitive effect may be because of the high conductivity of the cell culture medium and the small average size of the ASCs. Cell gradient measurements indicate that EIS could be used to detect the amount of cells in the sample. However, it seems that EIS would measure the cell amount indirectly because of cell metabolism and the cell culture medium.

Cell viability measurements proofed that EIS can distinguish living cells from dead cells, since the impedance decrease is 13 % due to cell death in a sample containing 0.5 million ASCs in clusters. The significance is statistically tested using t-test. Thus EIS could provide a tool for measuring cell viability in a non-invasive manner and without needing optical markers.

Altogether, EIS is an error sensitive measurement technique and some errors are not easy to notice during the measurements. The most important limitations of EIS measurements in this work are the relatively small number of cell samples and the use of long cables. Additional measurements are needed to assess the ability of measuring the amount of cells by EIS. For that purpose it would be good to have cells with more uniform size to be able to calculate the volume fraction of the cells accurately. The viability measurements should be proofed by measuring the EIS of separated samples encapsulated with a known amount of living and dead cells. In order to distinguish how major effect the cell culture medium has and if it covers the capacitive effect from cells, a blank GG hydrogel with encapsulated cells without inserting the cell culture medium could be measured.

EIT simulations have shown important features about the studied methods, the resistivity of the aqueous solution and the electrode locations that are important in planning the future measurements. It is important to have as much information as

possible of the sample in order to reconstruct EIT images. For this purpose two methods are studied: the opposite and the neighboring. The opposite method would be ideal for scoping the center parts of the sample. The neighboring method measurements would give data about the boundary regions of the sample.

The development of the EIT system is still in the beginning and this work provides initial information on how to carry on this development. First, the electrode supports are built according to the parameters obtained from EIT simulations. A Compromise for electrode location needs to be done because, in practice, changing electrode locations at the same measurement occasion would be very time consuming. Thus electrode separation of 1 mm and electrode distance of 0.5 mm from the sample would provide a good compromise for both the opposite and the neighboring methods. Next steps include practical measurements, image reconstruction first in 2D and then in 3D.

REFERENCES

[1] A. A. Appel, M. A. Anastasio, J. C. Larson, and E. M. Brey, “Imaging challenges in biomaterials and tissue engineering.,” *Biomaterials*, vol. 34, pp. 6615–30, Sep. 2013.

[2] E. Dawson, G. Mapili, K. Erickson, S. Taqvi, and K. Roy, “Biomaterials for stem cell differentiation.,” *Adv. Drug Deliv. Rev.*, vol. 60, pp. 215–28, Jan. 2008.

[3] N. E. Fedorovich, I. Swennen, J. Girones, L. Moroni, C. A. Van Blitterswijk, E. Schacht, J. Alblas, and W. J. A. Dhert, “Evaluation of Photocrosslinked Lutrol Hydrogel for Tissue Printing Applications,” *Biomacromolecules*, vol. 10, pp. 1689–1696, 2009.

[4] E. Barsoukov and J. Macdonald, Eds., *Impedance Spectroscopy : Theory, Experiment, and Applications*, 2nd ed. John Wiley & Sons, Incorporated, 2005, p. 615.

[5] S. Grimnes and Ø. G. Martinsen, *Bioimpedance & Bioelectricity Basics*, 2nd ed. Elsevier Ltd, 2008.

[6] B. Klösgen, C. Rümenapp, and B. Gleich, “Bioimpedance Spectroscopy,” in *BetaSys Systems Biology of Regulated Exocytosis in Pancreatic ß-Cells*, 2nd ed., B. Booß-Bavnbek, B. Klösgen, J. Larsen, F. Pociot, and E. Renström, Eds. Springer Science+Business Media, 2011, pp. 241–271.

[7] T. Sun, S. Tsuda, K.-P. Zauner, and H. Morgan, “On-chip electrical impedance tomography for imaging biological cells.,” *Biosens. Bioelectron.*, vol. 25, pp. 1109–15, Jan. 2010.

[8] H. Morgan, T. Sun, D. Holmes, S. Gawad, and N. G. Green, “Single cell dielectric spectroscopy,” *J. Phys. D. Appl. Phys.*, vol. 40, pp. 61–70, Jan. 2007.

[9] G. Mernier, N. Piacentini, R. Tornay, N. Buffi, and P. Renaud, “Cell viability assessment by flow cytometry using yeast as cell model,” *Sensors Actuators B Chem.*, vol. 154, pp. 160–163, Jun. 2011.

[10] C. Hildebrandt, H. Büth, S. Cho, Impidjati, and H. Thielecke, “Detection of the osteogenic differentiation of mesenchymal stem cells in 2D and 3D cultures by electrochemical impedance spectroscopy.,” *J. Biotechnol.*, vol. 148, pp. 83–90, Jul. 2010.

[11] D. Kloss, R. Kurz, H.-G. Jahnke, M. Fischer, A. Rothermel, U. Anderegg, J. C. Simon, and A. a Robitzki, “Microcavity array (MCA)-based biosensor chip for functional drug screening of 3D tissue models.,” *Biosens. Bioelectron.*, vol. 23, pp. 1473–80, May 2008.

[12] A. R. A. Rahman, J. Register, G. Vuppala, and S. Bhansali, “Cell culture monitoring by impedance mapping using a multielectrode scanning impedance spectroscopy system (CellMap).,” *Physiol. Meas.*, vol. 29, pp. 227–39, Jun. 2008.

[13] F. a Alexander, D. T. Price, and S. Bhansali, “From cellular cultures to cellular spheroids: is impedance spectroscopy a viable tool for monitoring multicellular spheroid (MCS) drug models?,” *IEEE Rev. Biomed. Eng.*, vol. 6, pp. 63–76, Jan. 2013.

[14] C. Canali, A. Heiskanen, H. B. Muhammad, P. Høyum, F.-J. Pettersen, M. Hemmingsen, A. Wolff, M. Dufva, O. G. Martinsen, and J. Emnéus, “Bioimpedance monitoring of 3D cell culturing-Complementary electrode configurations for enhanced spatial sensitivity.,” *Biosens. Bioelectron.*, vol. 63, pp. 72–9, Jan. 2015.

[15] P. Kauppinen, J. Hyttinen, and J. Malmivuo, “Sensitivity Distribution Simulations of Impedance Tomography Electrode Combinations,” *Int. J. Bioelectromagn.*, vol. 7, pp. 344–347, 2005.

[16] D. S. Holder, Ed., *Electrical Impedance Tomography: Methods, History and Applications*. IOP Publishing Ltd, 2005.

[17] P. Linderholm, L. Marescot, M. H. Loke, and P. Renaud, “Cell Culture Imaging Using Microimpedance Tomography,” vol. 55, pp. 138–146, 2008.

[18] S. U. Kim and J. de Vellis, “Stem cell-based cell therapy in neurological diseases: a review.,” *J. Neurosci. Res.*, vol. 87, pp. 2183–2200, Aug. 2009.

[19] “Regea.” [Online]. Available: http://www.regea.fi/stemcell.php?l=en. [Accessed: 31-Jul-2014].

[20] L. Ylä-Outinen, “Functionality of Human Stem Cell Derived Neuronal Networks - Biomimetic environment and characterization,” University of Tampere, 2012.

[21] S. Haimi, “Allograft Bone and Osteogenic Scaffolds Seeded with Human Adipose Stem Cells in Bone Tissue Engineering,” University of Tampere, 2008.

[22] E. R. Morris, K. Nishinari, and M. Rinaudo, “Gelation of gellan – A review,” *Food Hydrocoll.*, vol. 28, pp. 373–411, Aug. 2012.

[23] A. M. Smith, R. M. Shelton, Y. Perrie, and J. J. Harris, “An initial evaluation of gellan gum as a material for tissue engineering applications.,” *J. Biomater. Appl.*, vol. 22, pp. 241–54, Nov. 2007.

[24] R. López-Cebral, P. Paolicelli, V. Romero-caamaño, S. Begoña, M. A. Casadei, and A. Sanchez, “Spermidine-Cross-linked Hydrogels as Novel Potential Platforms for Pharmaceutical Applications,” *J. Pharm. Sci.*, vol. 102, pp. 2632–2643, 2013.

[25] C. F. J. Coombs, *Electronic Instrument Handbook*, 3rd ed. McGraw-Hill Companies, Inc, 2000.

[26] A. Beiser, *Schaum's Outline of Applied Physics*, 4 th. ed. McGraw-Hill Companies, Inc, 2009.

[27] *Compendium of Chemical Terminology Gold Book*. International Union of Pure and Applied Chemistry, 2014, p. 1670.

[28] H. Fricke, "A Mathematical Treatment of the Electric Conductivity and Capacity of Disperse Systems I. The Electric Conductivity of a Suspension of Homogeneous Spheroids," *Phys. Rev.*, vol. 24, pp. 575–587, 1924.

[29] V. Vermeeren and L. Michiels, "Evolution Towards the Implementation of Point-Of-Care Biosensors," in *Biosensors for Health, Environment and Biosecurity*, In Tech, 2011.

[30] D. M. Kirchmajer, B. Steinhoff, H. Warren, R. Clark, and M. in het Panhuis, "Enhanced gelation properties of purified gellan gum.," *Carbohydr. Res.*, vol. 388, pp. 125–9, Mar. 2014.

[31] P. Linderholm, R. Schoch, and P. Renaud, "Microelectrical Impedance Tomography for Biophysical Characterization of Thin Film Biomaterials," in *Transducers '03*, 2003, pp. 284–287.

[32] X. Huang, D. W. Greve, D. D. Nguyen, and M. M. Domach, "Impedance Based Biosensor Array for Monitoring Mammalian Cell Behavior," in *Sensors, 2003*, 2003, pp. 304–309.

[33] S. Montgomery, "Impedance measurement system for emryonic stem cell and emryoid body cultures," Georgia institute of Technology, 2008.

[34] R. Davalos and B. Rubinsky, "Electrical Impedance Tomography of Cell Viability in Tissue With Application to Cryosurgery," *J. Biomech. Eng.*, vol. 126, pp. 305–309, 2004.

[35] K. F. Lei, "Review on Impedance Detection of Cellular Responses in Micro/Nano Environment," *Micromachines*, vol. 5, pp. 1–12, Jan. 2014.

[36] R. Pethig, A. Menachery, S. Pells, and P. De Sousa, "Dielectrophoresis: a review of applications for stem cell research.," *J. Biomed. Biotechnol.*, Jan. 2010.

[37] R. Davalos and B. Rubinsky, "Electrical Impedance Tomography of Cell Viability in Tissue With Application to Cryosurgery," *J. Biomech. Eng.*, vol. 126, pp. 305–309, 2004.

[38] J. Malmivuo and R. Plonsey, *Bioelectromagnetism*. New York: Oxford University Press, 1995.

[39] J. L. Mueller and S. Siltanen, *Linear and Nonlinear Inverse Problems with Practical Applications.* SIAM Computational Science & Engineering, 2012, p. 351.

[40] P. Kauppinen, J. Hyttinen, and J. Malmivuo, “Sensitivity Distribution Visualizations of Impedance Tomography Measurement Strategies,” *Int. J. Bioelectromagn.*, vol. 8, p. VII/1 – VII/9, 2006.

[41] M. Michálek, J. Sedláček, M. Parchoviansky, M. Michálková, and D. Galusek, “Mechanical properties and electrical conductivity of alumina/MWCNT and alumina/zirconia/MWCNT composites,” *Ceram. Int.*, vol. 40, pp. 1289–1295, 2014.

[42] J. Sivula (PhD), BioMediTech, Tampere. Interview on 24.10.2014.

[43] R. Pethig and G. H. Markx, “Applications of dielectrophoresis in biotechnology,” *Trends Biotechnol.*, vol. 15, pp. 426–432, 1997.

[44] H. P. Schwan, “Electrode polarization impedance and measurements in biological materials,” *Ann. New York Acad. Sci.*, pp. 191–209, 2006.

[45] K. Shinyama and S. Fujita, “Study on the electrical properties of a biodegradable plastic,” in *Properties and Applications of Dielectric Materials*, 2003.

[46] “HF2IS Impedance Spectroscope,” 2014. [Online]. Available: http://www.zhinst.com/products/hf2is. [Accessed: 04-Nov-2014].

[47] “HF2 User Manual,” 2008. [Online]. Available: http://www.zhinst.com/products/hf2is. [Accessed: 04-Nov-2014].

[48] P. Linderholm, J. Vannod, Y. Barrandon, and P. Renaud, “Bipolar resistivity profiling of 3D tissue culture,” *Biosens. Bioelectron.*, vol. 22, pp. 789–96, Jan. 2007.

[49] P. Pissis and A. Kyritsis, “Electrical conductivity studies in hydrogels,” *Solid State Ionics*, vol. 97, pp. 105–113, 1997.

[50] B. Hildebrandt, P. Wust, O. Ahlers, A. Dieing, G. Sreenivasa, T. Kerner, R. Felix, and H. Riess, “The cellular and molecular basis of hyperthermia,” *Crit. Rev. Oncol. Hematol.*, vol. 43, pp. 33–56, Jul. 2002.

[51] J. Laaksonen and M. Hirsimäki, “Fysiikan oppilaslaboratorio Virheiden ja tulosten analysoiminen.” Tampereen teknillinen yliopisto Fysiikan laitos.

[52] A. Seppänen, L. Heikkinen, T. Savolainen, A. Voutilainen, E. Somersalo, and J. P. Kaipio, “An experimental evaluation of state estimation with fluid dynamical models in process tomography,” *Chem. Eng. J.*, vol. 127, pp. 23–30, Mar. 2007.

[53] D. V Hutton, *Fundamentals of Finite Element Analysis*. New York, USA: McGraw-Hill Companies, Inc, 2003.

[54] R. Seppänen, S. Tiihonen, H. Wuolijoki, M. Kervinen, J. Smolander, A. Haavisto, L. Karkela, and K. Varho, *MAOL-taulukot Matematiikka, Fysiikka, Kemia*, 2nd ed. Kustannusosakeyhtiö Otava, 2000.

[55] P. R. Roberge, *Corrosion Engineering*. McGraw-Hill Companies, Inc., 2008.

[56] H. Nyberg and K. Jokela, Eds., *Sähkömagneettiset kentät*. Säteilyturvakeskus, 2006.

[57] T. Meissner and F. J. Wentz, "The complex dielectric constant of pure and sea water from microwave satellite observations," *IEEE Trans. Geosci. Remote Sens.*, vol. 42, pp. 1836–1849, Sep. 2004.

[58] M. Bass, Ed., *Handbook of Optics: Volume IV - Optical Properties of Materials, Nonlinear Optics, Quantum Optics*, 3rd ed. McGraw-Hill Companies, Inc., 2010.

[59] "Complex Dielectric Constant of Water." [Online]. Available: http://www.random-science-tools.com/electronics/water_dielectric.htm. [Accessed: 26-Sep-2014].

[60] J. Parraga (MSc), BioMediTech, Tampere. Email discussion on 25.3.2014.

[61] R. Watling, "Why do bubbles form if a glass of water is left alone for a while?," *Scientific American*, 2006. [Online]. Available: http://www.scientificamerican.com/article/why-do-bubbles-form-if-a/. [Accessed: 20-Oct-2014].

APPENDIX 1: ORIGINAL DATA OF VIABILITY MEASUREMENTS

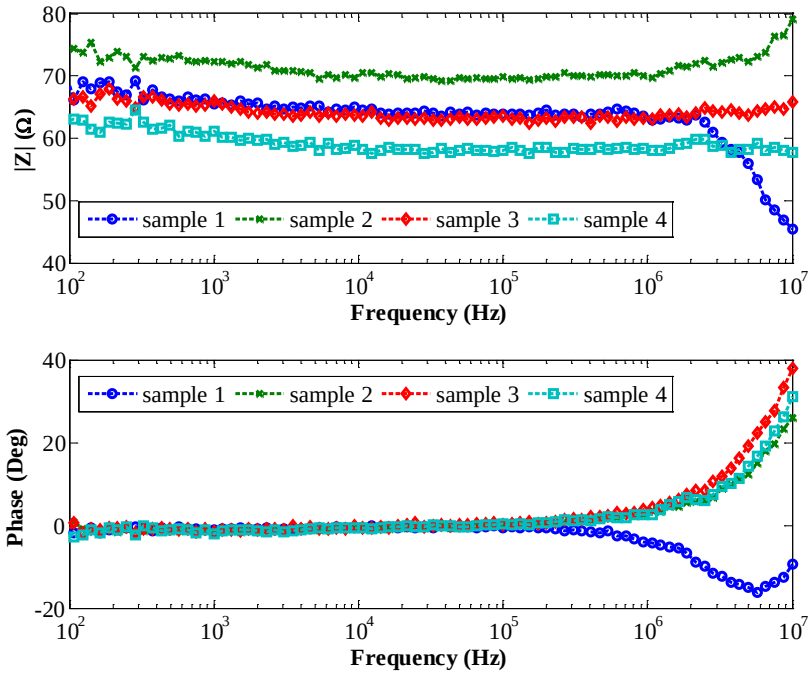

Figure A1.1 *Bode plot of 0.5 million ASCs in 1ml of GG-0.6SPM hydrogel before heat exposure.*

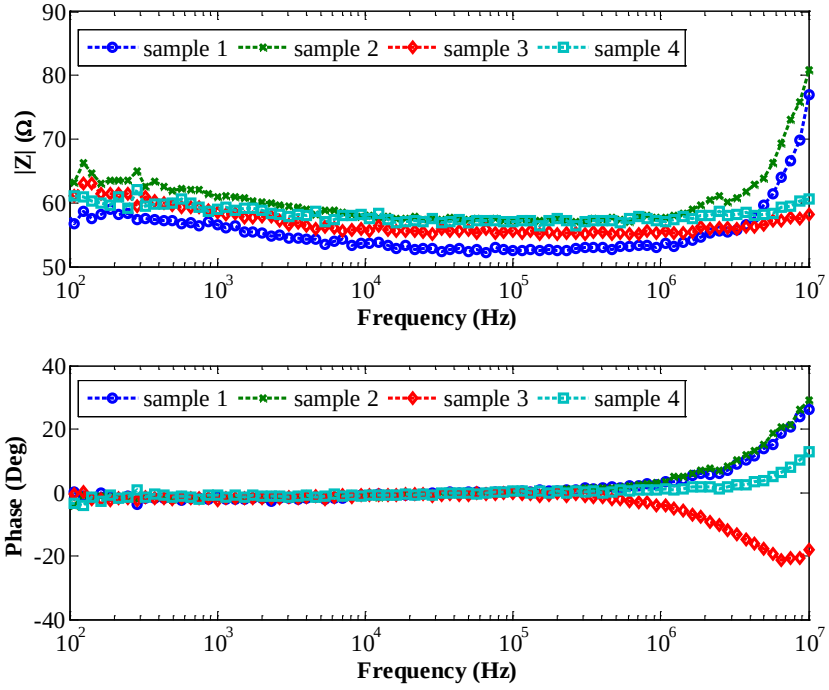

Figure A1.2 *Bode plot of 0.5 million ASCs in 1ml of GG-0.6SPM hydrogel after heat exposure.*

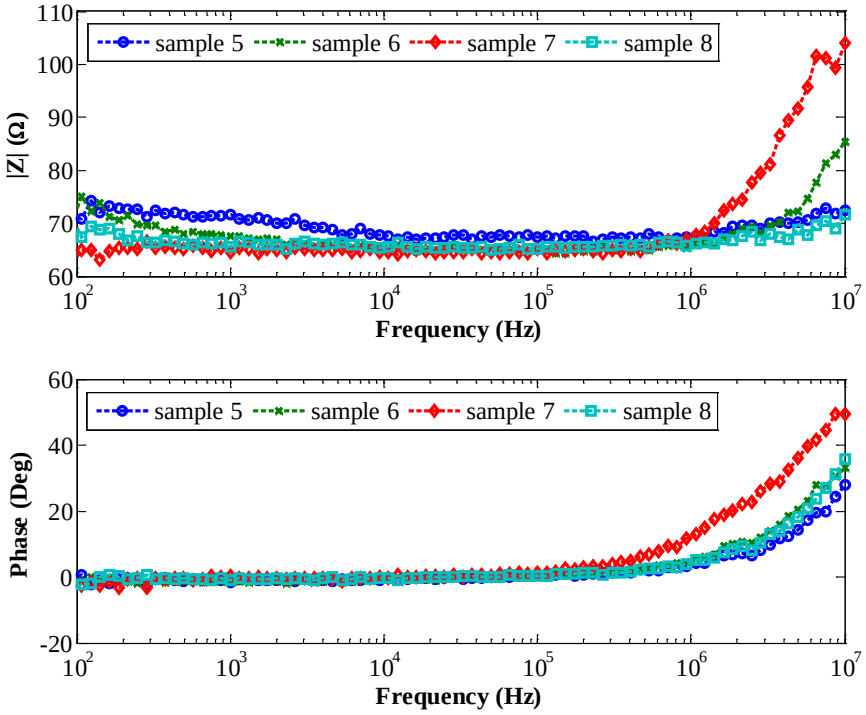

Figure A1.3 *Bode plot of bulk samples before heat exposure.*

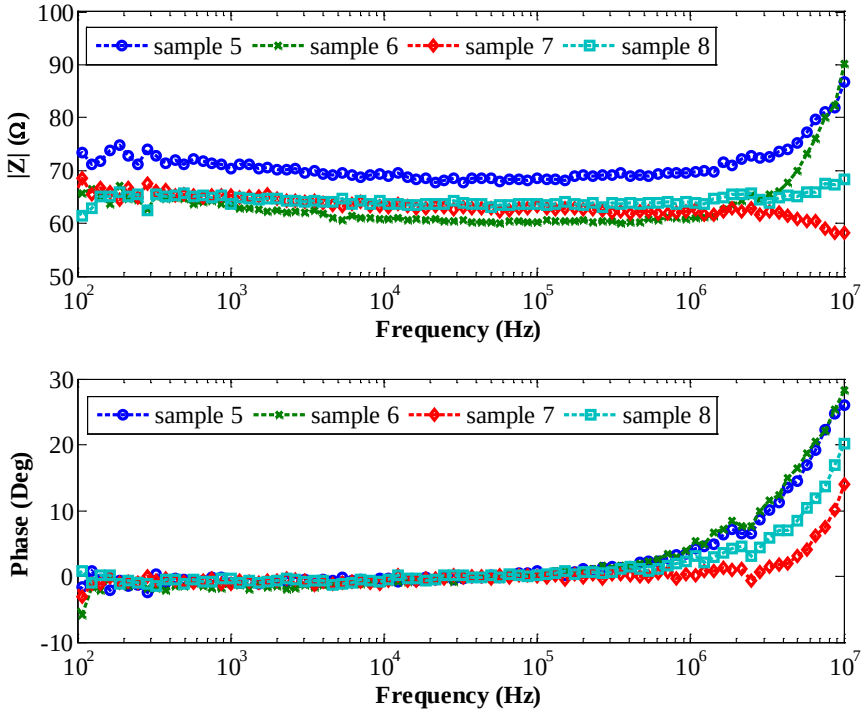

Figure A1.4 *Bode plot of bulk samples after heat exposure.*

APPENDIX 2: CURRENT DENSITY FIELDS OF EIT MODELS

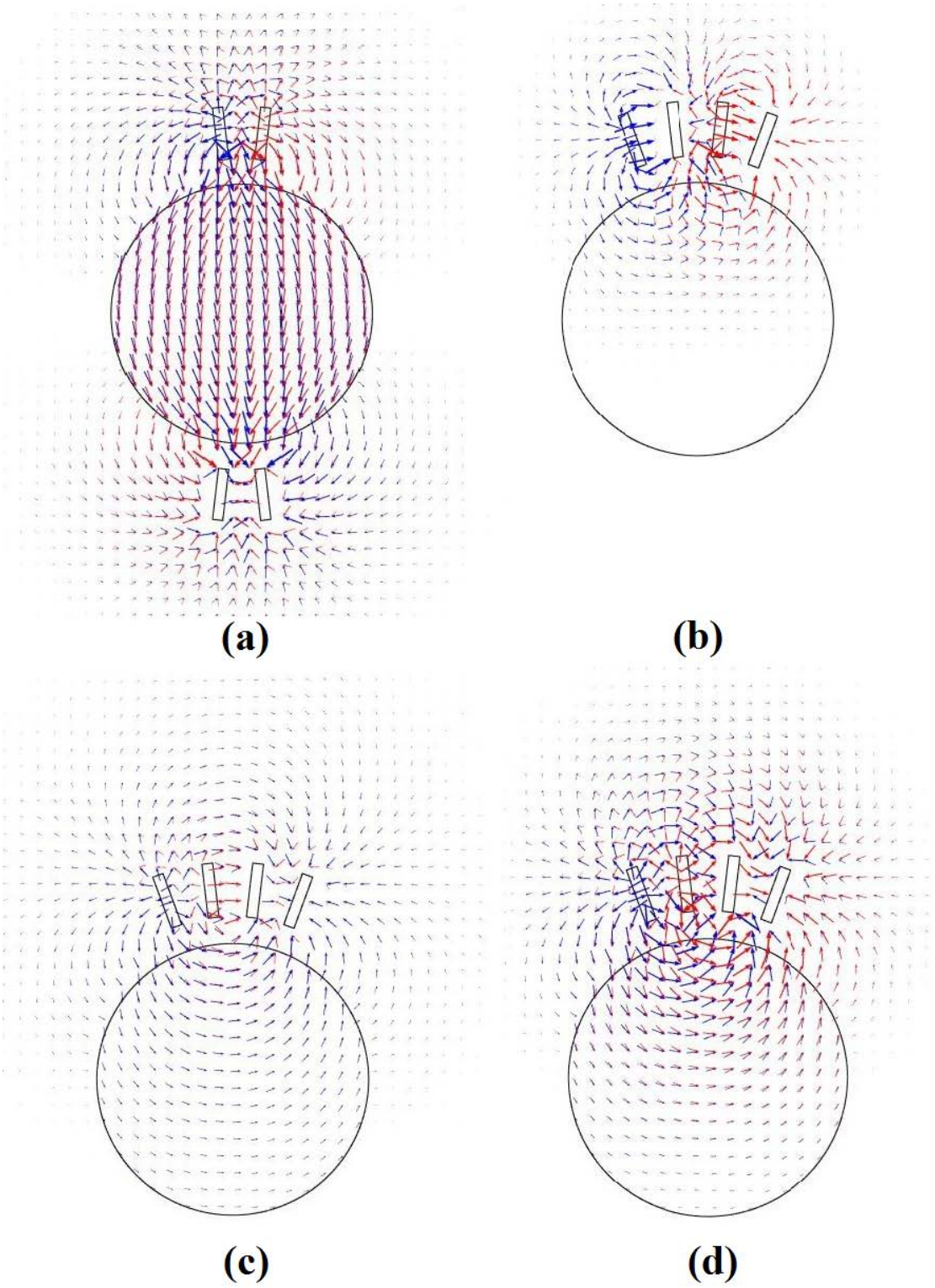

Figure A2.1. *Current density fields of each technique used in this thesis: (a) opposite, (b) next to, (c) edges and (d) every other. Distance between electrode tips and from electrodes to sample are 1 mm. Sample resistivity is 0.6 Ωm and aqueous solution resistivity is 30 Ωm. Sample diameter is 1 cm.*